MODIFICATION OF GOLD SURFACE BY LAYER-BY-LAYER REACTIVE COATING OF POLYESTER-POLYETHYLENEIMINE BASED GEL

A Thesis Submitted to the
Graduate School of
Izmir Institute of Technology
in Partial Fulfillment of the Requirements for the Degree of

MASTER OF SCIENCE

in Chemistry

by
Öykü YILDIRIMKARAMAN

July 2020
İZMİR

ACKNOWLEDGMENTS

There are several people without whom it would not have been possible to complete this master thesis and to whom I am grateful.

First of all, I would like to thank my supervisor Assoc. Prof. Dr. Ümit Hakan YILDIZ for his full support, expert guidance, understanding, and encouragement over the last years. His in-depth knowledge and patience made it possible to complete this thesis. I am extremely grateful for being part of a work team of his research group.

Also, I would like to thank Ufuk Saim GÜNAY and ITU group for the support of this work through supplying polyester type polymer.

I am very grateful to Sezer ÖZENLER for his great patience, and motivation at all times. Besides, I would like to thank Dilce ÖZKENDİR İNANÇ, Müge YÜCEL, Mustafa Umut MUTLU, Gündeniz AKKOÇ, Merve Beril DOĞDAŞ BAŞÇILAR and all members of the BioSens&BioApps and Biomimetics groups for their friendship and aids during my studies.

Finally, my sincere thanks to my parents Filiz & Ulvi YILDIRIMKARAMAN and my all family for supporting me spiritually throughout my entire study and encouraged my activities. And thanks my nephew, Ahmet Kuzey KARAKAŞ to being with me in this process.

ABSTRACT

MODIFICATION OF GOLD SURFACE BY LAYER-BY-LAYER REACTIVE COATING OF POLYESTER-POLYETHYLENEIMINE BASED GEL

Polymeric gels defined as soft and solid-like systems that enable to retain a large volume of solvent and their high molecular weight provides long-term stability without crystallization. Therefore, the use of polymeric gels in the fields of energy and sensor technologies has become advantageous. In this thesis, the polymeric gel is successfully synthesized on the gold surface by Aza-Michael addition reaction of the polyester scaffold with a triple covalent bond and branched polyethyleneimine which is a secondary amine source. The polyester-polyethyleneimine based gel was generated on the isocyanate functionalized gold surface by using the grafting-to methodology. The morphology of the surface and thickness of the coating can be adjusted by layer-by-layer reactive coating on the gold surface of polymer structures. Electroactive properties are acquired for different application areas of the synthesized gels. To provide modular electron transfer, polyethyleneimine was modified with ferrocene carboxaldehyde prior to obtaining gel on the surface. The gel interface on the gold surface will increase the surface area and activity due to its three-dimensional structure and adjustable morphology. The number of the immobilized structures, the electroactive species in a unit area and electron transfer increases. The modified electrode surfaces coating yields and electroactivity examined with electrochemical methods, Cyclic Voltammetry and Electrochemical Impedance Spectroscopy. The morphological properties investigated by Atomic Force Microscopy. Additionally, polyester-based gels lithium-ion conductivity was investigated. Dissociation of lithium perchlorate in the gel and enhancing the conductivity was investigated. Indium tin oxide coated glasses were used as an electrode to characterize lithium ion conductivity.

ÖZET

POLİESTER-POLİETİLENİMİN BAZLI JELİN KATMAN KATMAN REAKTİF KAPLAMA İLE ALTIN YÜZEYİN MODİFİKASYONU

Polimerik jeller yüksek hacimde çözücü tutabilen yumuşak ve katı benzeri yapılardır. Yüksek moleküler ağırlıkları, polimerik jellere kristalleşmeden uzun süreli stabilite sağlar. Bu nedenle polimerik jellerin enerji ve sensor teknolojilerinde kullanılması avantajlıdır. Bu tezde, üçlü kovalent bağ içeren poliester iskele ve ikincil amin kaynağı olan dallı polietilenimin Aza-Michael katılma tepkisi vererek altın yüzey üzerinde polimerik jel başarıyla oluşturulmuştur. İzosiyanat grupları ile fonksiyonlandırılmış altın yüzey üzerinde aşılama metodu ile poliester-polietilenimin bazlı jel oluşturulmuştur. Polimer yapıların altın yüzeyine katman katman reaktif kaplanması ile yüzeyin morfolojisi ve oluşturulan kaplamanın kalınlığı ayarlanabilinir. Sentezlenen jellerin farklı uygulama alanlarına yönelik elektroaktif özellikler kazandırılmıştır. Modüler elektron transferini sağlamak için, yüzey üzerinde jel elde edilmeden önce polietilenimin, ferrosen karboksaldehid ile modifiye edildi. Altın yüzeyindeki jel arayüzü, üç boyutlu yapısı ve ayarlanabilir morfolojisi nedeniyle yüzey alanını ve aktivitesini artıracaktır. İmmobilize yapıların sayısı, birim alandaki elektroaktif türler ve elektron transferinin artar. Modifiye edilmiş elektrot yüzeylerin kaplama verimleri ve elektroaktiviteleri elektrokimyasal yöntemlerle incelenmiştir, Döngüsel Voltametri ve Elektrokimyasal Empedans Spekstroskopisi. Morfolojik özellikler Atomik Kuvvet Mikroskobu tarafından inclenmiştir. Ayrıca, polyester bazlı jellerin lityum-iyon iletkenliği de araştırılmıştır. Jel içindeki lityum perkloratın ayrılması ve iletkenliğin arttırılması araştırıldı. Lityum iyon iletkenliğini karakterize etmek için indiyum kalay oksit kaplı camlar elektrot olarak kullanıldı.

TABLE OF CONTENTS

LIST OF FIGURES

Figure **Page**

LIST OF TABLES

Table **Page**

LIST OF ABBREVIATIONS

AFM …..……. Atomic Force Microscopy

PEI …… Polyethyleneimine

BPEI ……. Branched polyethyleneimine

Fc …… Ferrocene

EFM …….. Electrostatic Force Microscopy

CV …….. Cyclic Voltammetry

EIS ……...… Electrochemical Impedance Spectroscopy

FTIR …….. Fourier Transform Infrared Spectroscopy

ATR ……. Attenuated Total Reflectance

PC …….……. Propylene Carbonate

EC ……..…… Ethylene Carbonate

EN……...…… Ethylenediamine

EAP……...…….…… Electroactive polymer

LbL…….……Layer-by-Layer

EtOH……....Ethan

CHAPTER 1

INTRODUCTION

1.1. Scope of the Thesis

Polymeric gels are attractive due to their inherent physical and chemical properties. Here we synthesized polymeric organogels via Aza-Michael addition reaction of polyester scaffold and secondary amine consisting polymer. The ultra-fast gel formation process was carried out without using any initiator. The electroactive properties investigated as an ion conductance and modular electron transfer. Prepared polymeric gels were used as an electrolyte to modify the interface of the electrodes. The gel formation process was carried out to adapt to various surface application areas with two different methods, bulk gel, and surface grafting. Prepared gels chemical and morphological structures examined by FTIR, CV, and AFM.

1.2. Gel Definition

The gel and its form were very first defined at the beginning of the 19th century. The first gel term was used by Thomas Graham who defined gel with a simple “inversion test”. According to Graham, the gel should support its weight without falling. [1] The most general and accepted definition of the gel was made in 1974 by Nobel prized chemist Paul Flory; Gels composed of a two-component and colloidal dispersion with a continuous structure with macroscopic dimensions that is permanent on the timescale of the experiment and is solid-like in its rheological behavior. [2]

The composition of a gel is a combination of liquid (fluid component) and solid (gelling agent) matter. Also, they are defined as a type of non-Newtonian fluid. There are 3 different steps in the gelation procedure respectively, these are swelling, syneresis, and aging. The change in any of these three steps changes the properties of the gel as well.

Today, due to the gels' flexibility, low weight, and the ability to work in low volumes, their applicability in many areas increases.[1, 3-5]

1.3. Classification of Gels

A gel consists of both a 3D network and a medium. Therefore, the gels classified into two groups as their medium or source.[1, 6] Also, gels can specifically be classified by their crosslinking, types of medium, size of gel configuration, and, as well as whether they are natural or artificial (synthetical). [4, 5] In this case, a gel can be included in more than one class. Figure 1.

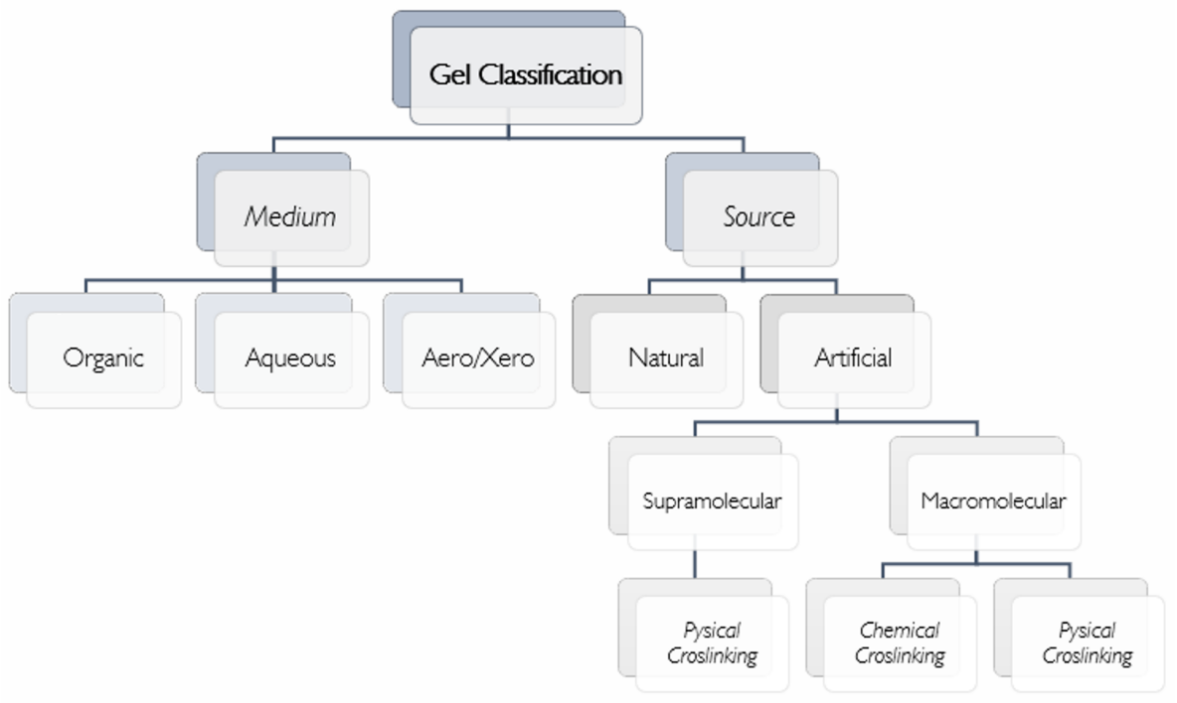

Figure 1. Classification of gels

Nowadays, especially gelling agents or gelators used as a source in gel components can be approached in two groups. These are low-molecular-weight gelators and interface gelators.[7] Low-molecular-weight gelators are small molecules that form a 'supramolecular' gel through non-covalent interactions. Because of their high

biocompatibility, low molecular weight gelators are used in medical applications, tissue engineering, drug delivery, and many other applications. [8-12] Polymeric gelators form the sample propagation network of long-chain polymer molecules necessary for gelation by covalent or non-covalent crosslinking. These gelling agents possess stable gel systems by reducing the interfacial and surface tension, thus increased the viscosity of the liquid medium.[5, 6] The polymeric gelators have been found that induced the gelation which leads to gelation even at low concentrations and comparatively high mechanical strength more than low-molecular-weight gelators. Because of these properties, they are preferred to be used in food, cosmetics, medicine, sensor, and energy storage systems.[5, 13, 14]

The most important factor that determines the structure and properties of the gel is the external solvent phase. The organogel is defined as a semi-solid material with a (nonpolar) liquid organic phase entrapped in a cross-linked network. Polymeric organogels are obtained by combining polymeric networks with an organic liquid medium.[15, 16] The polymeric organogels has various application fields such as drug delivery systems, pollutants removal, and supramolecular electronics, and for developing soft-optical devices, CO2 sorbents, chemical sensors.

1.4. Electroactive Polymer Gels

The gels are attractive since because they have a unique approach to the conventional properties of matter, such as mechanical and thermal properties, and rheological behaviors. Besides, the polymeric organogels have opportunities to customization for the specialty of the usage field in such a manner that electrical conductivity, photoconductivity, optical effects, and dielectric properties, by polymers behaviors. The exhibiting electrical activity or responsive to electrical stimuli is one of these features.[5] Electroactive polymeric systems comprise active polymers such as piezoelectric materials as well as polymers can be used in passive positions such as changing dimension or shape in response to stimuli. Thus, electroactive polymeric materials can be divided into two: ionic, which is electrically induced to transport ions and electronics, which is activated by being affected by the electric field. [17]Figure 2 shows the classification of electroactive polymers and their sub-categories.

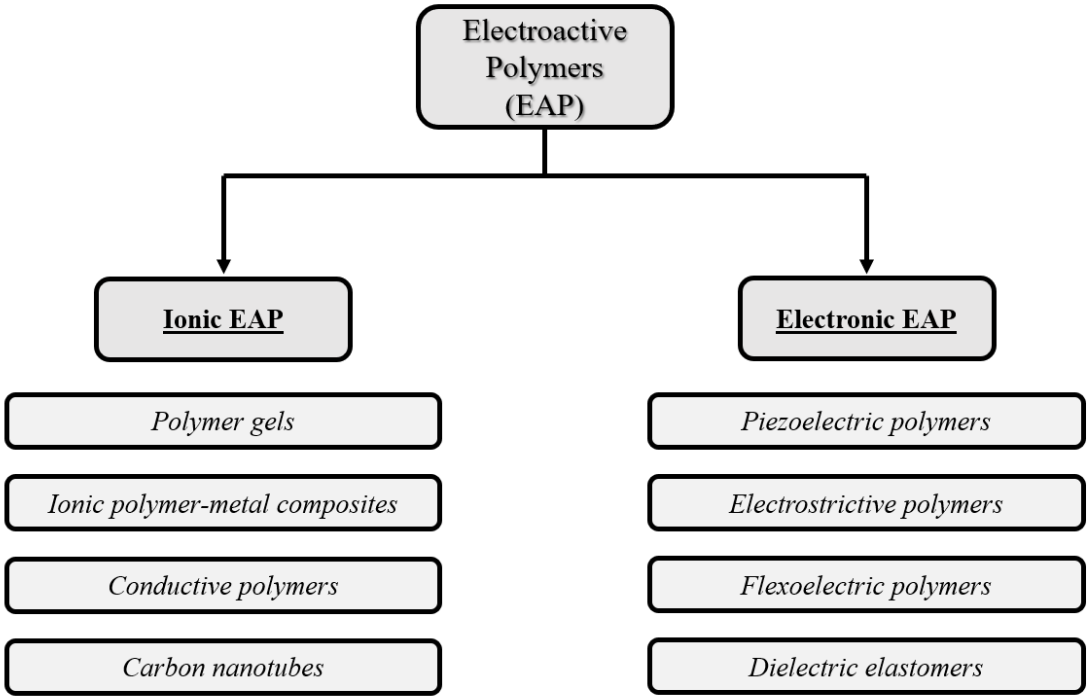

Figure 2. Schematic classification of electroactive polymers and their sub-categories. (re-arranged from; [17])

1.5. Application of Electroactive Polymer Gels

The electroactive polymer gels have a wide range of application fields and most are used as an electrolytic separator or supporting matrix. The most important application fields are energy storage devices such as batteries, solar cells, supercapacitors. Another most used areas are sensor technologies. Some of the other usages are catalytic membranes, drug release in biomedicine, light moderators, and actuators that convert electrical energy into mechanical work. Figure 3. [1, 17-19]

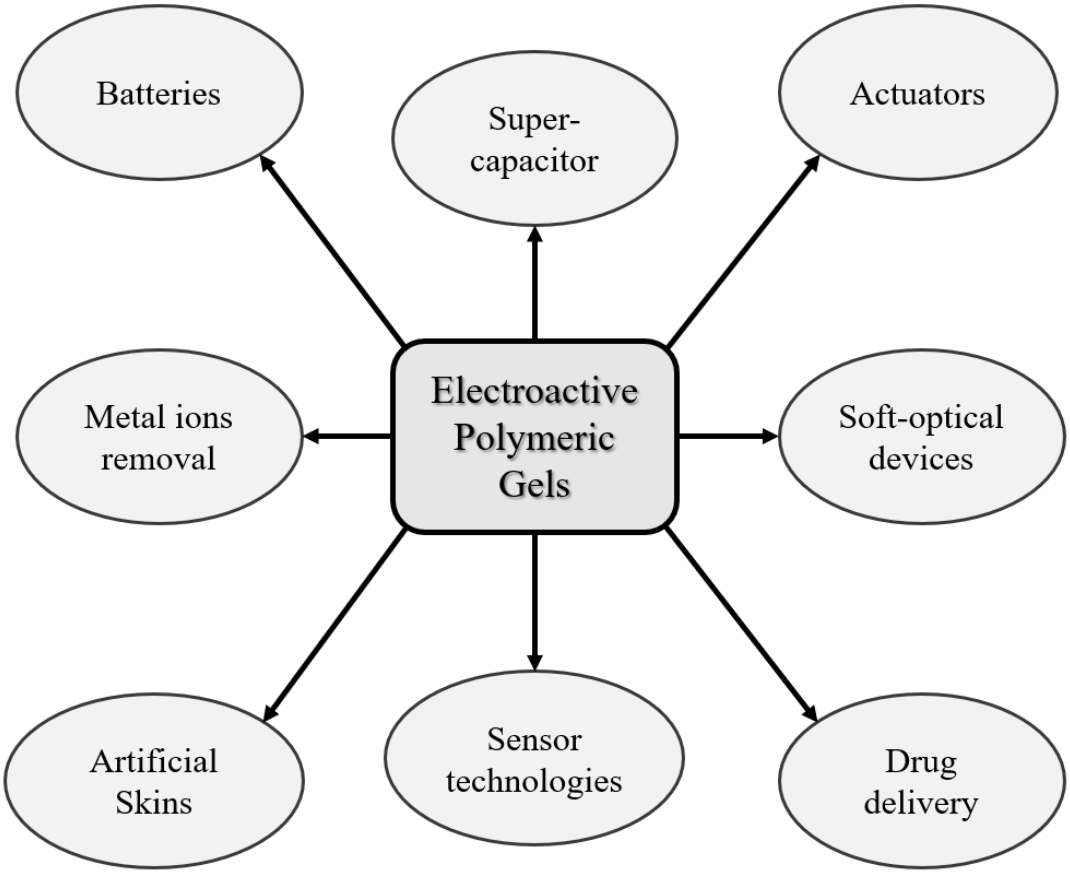

Figure 3. Schematic illustrations of applications of electroactive polymeric gels.

1.5.1. Lithium-Ion Based Energy Storage Devices

With the development of portable electronic devices, new types of resources have been produced to cater to the energy needs of these devices. Nowadays, at many battery and capacitor, the gel polymer electrodes with ionic liquid that contains lithium salt are used. Referring to the difference between battery and capacitor; while the power of the battery is produced by chemical reaction, the storage of the power in the capacitor and keeping it in an electric field are in the foreground. The battery can produce more energy for longer periods than a capacitor, but the capacitor can discharge higher current in a short period than a battery, even if it stores much less potential which is ideal when the higher current is required. The new generation supercapacitors have short charging times, a very long lifetime, and high energy densities compared to capacitors. The increase in the volumetric capacities of the supercapacitors has been promising that the energy

storage capacity can be compared to the batteries. Lithium-ion capacitors are innovative next-generation electricity storage devices. Ionically electro-activated polymeric gels usually composed of ionic liquids, besides that ionic additives can be also provided by salts in organic solvents is an option. The enhancement of lithium-ion conductivity in organogels opens a new path to make electrochemical energy storage.[1] The market for lithium-ion capacitors offers a wide range of applications including hybrid automotive and renewable energy.

1.5.2. Biosensors

Biosensors are analytical devices composed of recognition elements (receptor) and a transducer to detect the target analyte. According to their signal transduction or receptor, the biosensors classified as; electrochemical biosensors, optical biosensors, piezoelectrical, and thermal biosensors. Last few decades, the polymeric gels have a significant role in the development and fabrication of the biosensors. The electroactive polymeric gels mainly used as a supporting matrix in the electrochemical biosensor. The bio-element loading capacity of the supporting matrixes has a major role in interaction with the biological medium for biosensor applications. The bio-element loading capacity is directly affected the amplification degree of signal, signal-to-noise ratio, speed of propagation to the transducer, and indirectly affects both the area and size of the electrode. The bio-element loading can be increment achieve by using gels to increase the surface area of the sensor.

1.6. Surface Functionalization

Surface modifications carried out with organic-based structures containing high reactivity functional groups provide both macroscopic and nanometrically adjustable surfaces with inorganic, organic, and especially biological materials.[20-23] The development of the macromolecular surface science opens the way of using polymeric structures to modify the surface of materials.

Surface modification with polymeric structures such as surface grafting and layer by layer (LbL) assembly is important for biosensor applications in biology and

biochemistry at the characterization of interactions between biomolecules and cell surface receptors as well as protein electron transfer.[24-26] Modifications associated with polymeric structures are used as modulating interactions with the sensor interface, harmonious integration of nanostructures with live cells, and facilitating interfacial electron transfer (ET).[27-29] Thus, surfaces containing basic components for the rational design of complex arrays to be used in the field of nanoscience and technology, including optical, electrochemical sensor applications, and applications such as nano-electrochemistry and molecular electronics, are easily obtained.[30]

Besides of that, the nano-sized gels that are functional colloids with porous structure and swelling in aqueous medium but not disperse. Their tunable morphology, high porosity, and a unique capability to adjust their shape and dimensions increased interested in their usage of optoelectronics, biosensors, and energy storage devices.[31] The rationally designed nanogels provide an advantage in subjects that have an important role in the biosensor field, such as increasing the biocompatibility of the electrode, creating protective layers to control diffusion, controlling electron transfer, and improving probe immobilization efficiency.[32-34] Qu, F. et al. prepared a high amount of ferrocene-modified nanogel in the biosensor which developed for the electrochemical detection of glucose. The high sensitivity, wide linear range, short response time, and good stability were obtained due to improved enzyme loading and efficient electron transfer. However, in the study, the nanogel was not covalently attached to the electrode surface, so the nanogel surface interaction is not strong.[35] Freeman, M. et al. developed a biosensor that contains gold nanoparticle supported xerogel matrix to electrochemical detection of glucose. The xerogel matrix with gold nanoparticle additive, provided twice the linear range, improved degree of sensitivity, and faster response time accompanying long-term stability.[36]

1.6.1. Grafting

The polymer grafting becomes an important approach to functionalize the surfaces. Grafted polymers also called “polymer brushes”, “tethered polymer chains’’ or ‘‘end-grafted polymers’’ are tethered by one end to the surface.[37, 38]The characteristics of these layers modulate at the micro/ nanoscale of the surface properties without altering their bulk properties by controlling the grafting reaction conditions. Thus, surface grafting

methods provide a simple and efficient way to fine-tune the physical and chemical properties of the material interface.[39, 40]

In general, polymeric structures are attached to metal and semiconductor surfaces using methods such as chemisorption, covalent grafting, and physical adsorption. Physical adsorption results in an immobile polymer layer with limited stability and therefore less used than the other two methods.[41] The covalent grafting method for generating polymer brushes consists of two approaches: ‘‘grafting-to’’ and ‘‘grafting from’’. The “grafting from” technique involves the sequential growth of the monomers and initiates the polymerization from the previously activated substrate surface. However, the characterization of grafted chains is difficult. In contrast, the “grafting to” technique, pre-synthesized polymers tethered to the previously modified substrate surface.[38-40] Grafting the end-functional polymer with complementary functionalize groups on the surface via a chemical reaction (usually covalently bond) can be performed in a solution of the polymer or from the polymer melt.[42] However, the "grafting to" method is a self-limited process because of the steric hindrance of the deposited polymers. The grafted to be polymer reactive end-chains must first diffuse through to reach the complementary ends of the surface. This excluded volume region (barrier) become more distinct as the tethered polymer chain number increased. To prevent this behavior, a concentrated polymer solution used for grafting instead of the polymer melt.[37] Thereby, the morphology of the grafted layers generally depends on the intensity of the polymer solution and the grafting time. The short grafting times results in an island like structures on the surface. The major advantage of the “grafting to” method provides an opportunity to characterize the polymer via various chemical and physical methods. So, this approach yields a well-defined grafted polymer brush. Additionally, this method is less challenging over the “grafting from” method since it does not elaborate procedures. [40]

Moreover, polymer grafted surface can be achieved in either single or multiple steps.[40] Surface-initiated polymerization (SIP) based on radical chemistry is commonly used in the "grafting from" method.[43] Various techniques are commonly used for grafting polymers to surfaces, both for “grafting to” or “grafting from” strategies. Among these techniques, the most used, i.e. Atom Transfer Radical Polymerization (ATRP) and Reversible Addition-Fragmentation chain Transfer radical polymerization (RAFT). Atom transfer radical polymerization (ATRP) is one the most widely used method for both “graft from” and “graft to” techniques.[44]

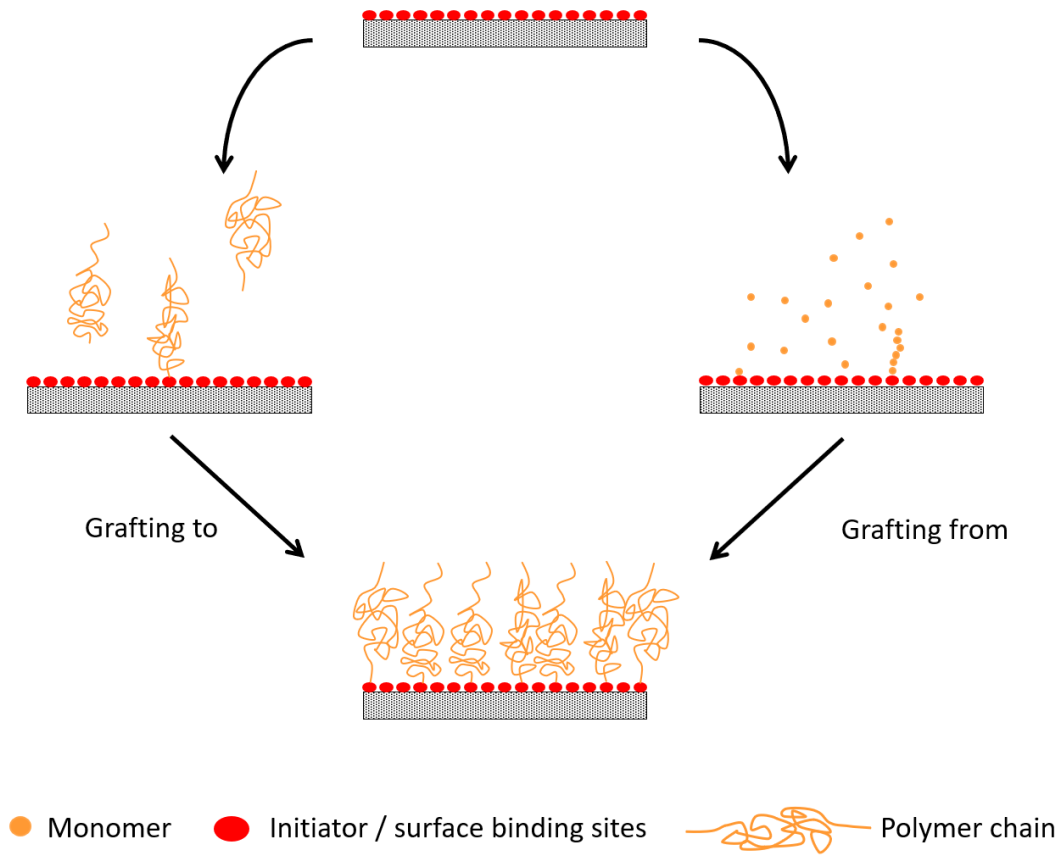

Figure 4. Schematic illustration describing the surface grafting strategies ("grafting-to" and "grafting-from" approaches)

Effective methodologies have been developed since the main difficulty in surface-based sensor applications is the irreversible adsorption tendency. Methods such as surface-initiated atom transfer radical polymerization (SI-ATRP) and activators regenerated by electron transfer (ARGET) ATRP are applied to create modified surfaces with bio-repellent polymers.[45-47] Although SI-ATRP and SI-ARGET ATRP methods are an effective methodology to replace the surface of metals, semiconductors as well as high dielectric metal oxides, the methods still require inconvenient polymerization steps that can be considered disadvantageous for practical biosensor applications.[48] However, degase steps are known to have disadvantages of SI-ATRP, which limits applicability. Therefore, recently, oxygen tolerant methodologies have emerged as an alternative to SI-ATRP. Yeow, J. et al compiled studies that highlight the pros and cons of recently controlled oxygen-tolerant controlled radical polymerization methodologies.[49] Nevertheless, both surface modification methods contain complex steps and do not offer practical solutions for wide-area applications.

1.6.2. Layer by Layer

In addition to grafting methodologies, multilayer thin-film depositions also alternative for surface modifications. The layer-by-layer assembly method (LbL) widely used to construct various functional ultrathin films in surface modification. Also, this method provides superior nanometer-scale control over film thickness and compositions for versatile applications.[50-52] The LbL assembly is a common method for coating substrates with polymers, colloids, biomolecules, nanoparticles, carbon nanotubes, dendrimers, enzymes, polymer micelles, and even cells. The multilayer thin film surface generates by the deposition of mutually attractive structures on the substrate via electrostatic interactions, hydrogen bonding, biospecific interactions, guest-host interactions, or other secondary interactions. [53-56]

The ionic forces most often used in modern LbL assembly to design functionalized surfaces. This LbL assembly approach requires a charged surface and then first coating layer opposite charged polymer which entropically favored on the surface. Also, non-ionic interactions like H-bond between hydrogen bond donor/acceptor polymers often used. However, the intrinsic properties of polyelectrolytes such as charge density influence the stability. Besides both kinds of interactions can easily disrupt by environmental conditions like pH, ionic strength, and temperature. The low stability often results in a change of structure and functionality of the coated thin film or resulting in a film degradation.[54, 55, 57]

The covalent layer by layer assembled thin films provides high stability against multivalent weak interactions due to covalently cross-linked polymer networks. There are two strategies to form a covalent assembly of LbL films. They are “post covalent conversion” and “consecutive covalent fabrication”. The post covalent conversion strategy refers to firstly building multilayer with a noncovalent interaction and then provide sufficient reaction conditions to form covalent bonds. Additionally, it requires a multiple charged or polar group in each building unit. In the consecutive covalent fabrication, the LbL film constructed directly using covalent reactions. The consecutive covalent LbL fabrication method allows small molecules included in multilayers as a building unit compared to post covalent conversion. Therefore, small molecules provide a stable linkage between layers. This results from insufficient charges of small molecules that prevent non-covalent assemblies.[53]

CHAPTER 2

MATERIAL & METHODS

2.1. Materials

11-mercapto-1-undecanol (97%, Sigma Aldrich), Polydimethylsiloxane (Sigma Aldrich) used for gold surface passivation, and preparation of PDMS stamp. Hexamethylene diisocyanate (HDI) (≥99.0%, Acros Organics), Dibutyltin dilaurate (DBTDL) (95%, Sigma Aldrich) used for gold surface post-functionalization. Branched polyethyleneimine (BPEI) (Mw ~25,000, Sigma Aldrich), Ethylenediamine (for synthesis, Merck) used for gelation. Ferrocene carboxaldehyde (98%, Sigma Aldrich) and Sodium borohydride (%90, Sigma Aldrich), Diethyl ether (Sigma Aldrich) used in the synthesis of ferrocene modified BPEI. Lithium perchlorate (99.99%, trace metals basis, Sigma Aldrich) used as an electrolyte salt. Potassium ferrocyanide (Sigma Aldrich), Potassium ferricyanide (III) (Sigma Aldrich) used as a redox couple. Di-Sodium hydrogen phosphate heptahydrate (ACS reagent, Sigma Aldrich), Sodium dihydrogen phosphate dihydrate (ACS reagent, Sigma Aldrich) used for the preparation of phosphate buffer solution. Propylene carbonate (anhydrous, 99.7%, Sigma Aldrich), Ethylene carbonate (98%, Sigma Aldrich), Acetone (99.5%, Sigma Aldrich), Ethanol absolute anhydrous (ACS reagent, Carlo Erba), Chloroform (99-99.4%, Sigma Aldrich), Methanol (Sigma Aldrich) used as a solvent. Hydrogen peroxide (%30, Merck) and Ammonium hydroxide solution (25-30% NH_3 basis, Sigma Aldrich) used in RCA cleaning, Chloroform-d (99.8%, Merck) used for 1H NMR analysis.

2.2. Michael Addition & Gelation

The Michael addition reaction is a nucleophilic addition of activated olefins and alkynes that contains electron-withdrawing groups to nucleophiles. The Michael addition reactions have a high functional group tolerance, reaction efficiencies, and favorable at

mild conditions. Thus, important for both synthetic and organic polymer chemistry. The Michael additions are used in chain growth polymerizations and the synthesis of linear, graft, hyper-branched, dendritic, and network polymers. [59] The polyester scaffold (P1) has an electron-deficient triple bond that used as Michael acceptor precursor for Aza- and Thiol- Michael addition reactions. The polyester scaffold has two electron-withdrawing carbonyl groups that connected to the alkyne that causes higher electron deficiency at triple bond. [60] The primary amines used as a nucleophile, Michael donor. Gunay et al., reported that primary amines show efficient functionalization within 2 minutes to generate a gel with P1. Also, they reported that reaction efficiency does not change when the reaction time gets longer. Moreover, alkyne takes place in a protic solvent (methanol, ethanol or water), the Z-isomer would be the major product, whereas the E-isomer would be the major product when the reaction takes place in an aprotic solvent (DMF, THF, CHCl3, etc.), regardless of amine type. [61]

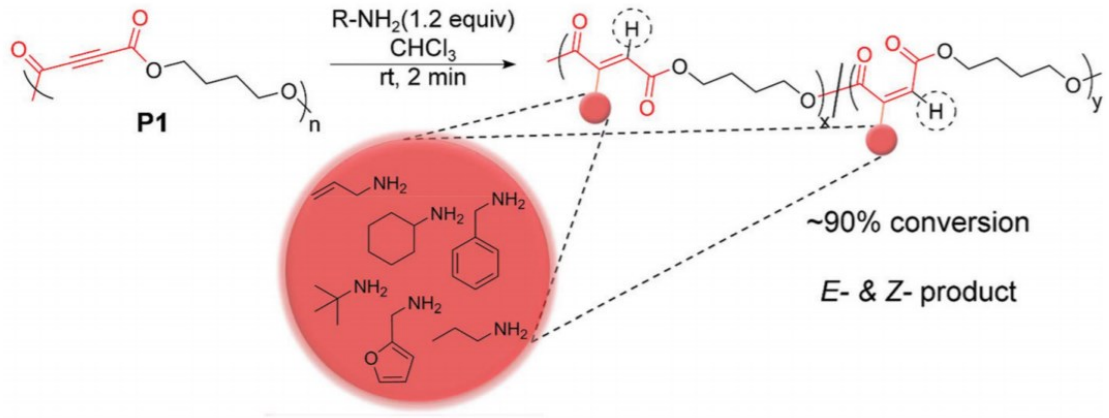

Figure 5. General representation of amino-yne reactions using primary amines. (Source:[61])

2.3. Sequential Reaction of Polyester with Electron Deficient on Gold Surface

It showed that the gold surface will be functionalized with hexamethylene diisocyanate (HDI) monomer, and then branched polyethyleneimine (PEI) and polyester

scaffold (P1) reacted with high efficiency on the gold surface, respectively. To observe optical and height differences on the gold surface, it was pacified with thiol-containing agents before the gold nanogel acquisition. Then, two steps of polymer reaction (PEI / P1) were applied to form a nanogel on the golden surface. Furthermore, since the interaction of the nanogel with the electrolyte solution (electrochemical measuring medium) will be higher compared to monolayer interfaces, electron transfer will be performed in a more efficient yield and a biosensor platform with the potential to reach the low limit of detection will be obtained. The idea of the presence of post-functional groups not only on the interface but also within the three-dimensional structure is provided by obtaining various loop numbers on the gold surface, thus providing an electroactive nanogel interface.

2.3.1. RCA Cleaning

Gold surfaces will be cleaned with the RCA cleaning method. In the method, the surface containing gold, distilled water, 30% hydrogen peroxide, 27% ammonium hydroxide (5: 1: 1 by volume) is kept at 80 ° C for approximately 30 minutes and the surfaces will be washed with plenty of distilled water.

2.3.2. Gold Substrate Passivation

The gold substrate passivation was applied by using 11-mercapto-1-undecanol. Polydimethylsiloxane (soft lithography - PDMS) stamp incubated in 1mM 11-mercapto-1-undecanol in the ethanolic solution for five minutes and stamp was dried by a jet of nitrogen gas. Then, the stamp placed on the gold substrate by applying slight pressure to ensure good contact between PDMS and surface.

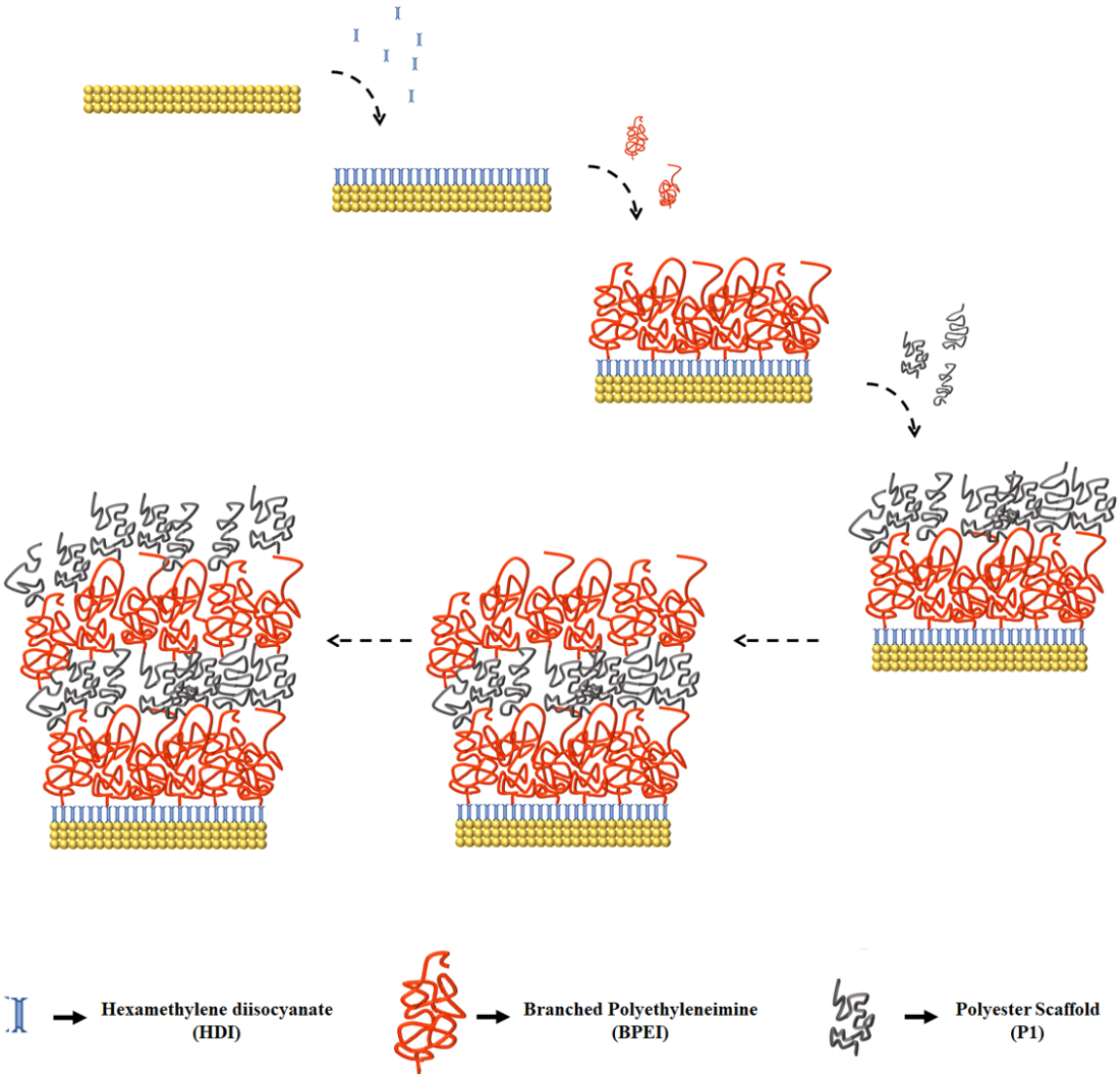

Figure 6. Schematic illustration of the process of 5-step LbL polymer assembly to form a gel.

2.3.3. Fc-BPEI Synthesis

The branched polyethyleneimine modified with ferrocene carboxaldehyde (Fc-BPEI) was synthesized as described elsewhere.[63] According to the ferrocene carboxaldehyde amount, the varying proportion of Fc-BPEI was synthesized (10%). The modification yield of Fc-BPEI was obtained by NMR.

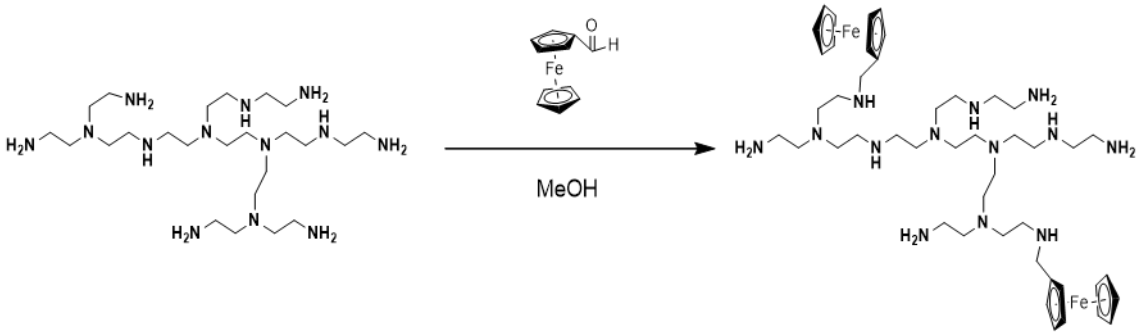

Figure 7. Reaction mechanism of branched polyethyleneimine (BPEI) and ferrocene carboxaldehyde (Fc).

In a round-bottom flask, 0.287 g of BPEI was dissolved in excess (~5 mL) of methanol, and a solution of 0.05 g (0.23 mmol) of ferrocene carboxaldehyde dissolved in excess (~0.5 mL) of methanol was added to it dropwise under constant agitation and in an ice bath. Dark red (tile) colored solution was obtained. The solution was stirred for about 2 hours. Then, sodium borohydride (0.015 g, 0.4 mmol) was added to the solution, and stirring was continued for 1 hour. Meanwhile, the color of the solution changed from dark red to orange/yellow. Finally, the methanol was removed under vacuum, and the residue was extracted overnight with diethyl ether to remove any nonreacted aldehyde and ferrocenylmethanol. The ether was then decanted, and the residue was washed with diethyl ether. The washing process with ether was continued every 2 hours, about 3 times. Then, the solvent removed under vacuum to give 10% of Fc-BPEI. The 1H-NMR spectra in deuterated chloroform were compared with reference spectra which were taken from literature. [63]

2.3.4. Electroactive nanogel synthesis on the gold surface

After the gold substrate RCA cleaning, nanogel formation will be performed by the incubation method. The first stage is incubation temperature (30 - 50 ° C) with hexamethylene diisocyanate (HDI) (50 mM - 250 mM) in the presence of dibutylindylainate (BDTL) catalyst (45 × 10-3 mM - 450 × 10-3 mM) in gold surface acetone. It is prepared to depend on the duration (15 - 30 minutes). At this stage, the two isocyanate (NCO) groups present in HDI tend to interact equally with the gold surface

(Fug et al., 2014). Thus, it is thought that an NCO group that does not interact on the surface is obtained at the end of the incubation.[47] After incubation, the gold surface is washed with copious chloroform. As a result of this process, only physically or chemically adsorbed diisocyanate groups are expected to remain on the gold surface.

As a second step, it is applied depending on the incubation temperature (30 - 50 ° C) and duration (15 - 30 min) of polyethyleneimine (PEI) (0.02 - 0.04 mM) in the presence of chloroform of gold substrates. At this stage, as a result of the reaction of the -NCO groups and PEI on the surface, urea groups are formed, and PEI is covalently bound to the surface. Subsequently, the polyester substrate in the presence of gold substrate chloroform (2 - 4 mM) is applied depending on the incubation temperature (30 - 50 ° C) and duration (15 - 30 min). At this stage, the polyester scaffold reacts with PEI and is covalently bound. As a result of these processes, a urea and polyester scaffold covalent bonding has occurred on the surface and in this research proposal, this process is expressed as a loop. After applying the desired number of cycles, the resulting nanogel is washed in the presence of copious chloroform and dried under nitrogen.

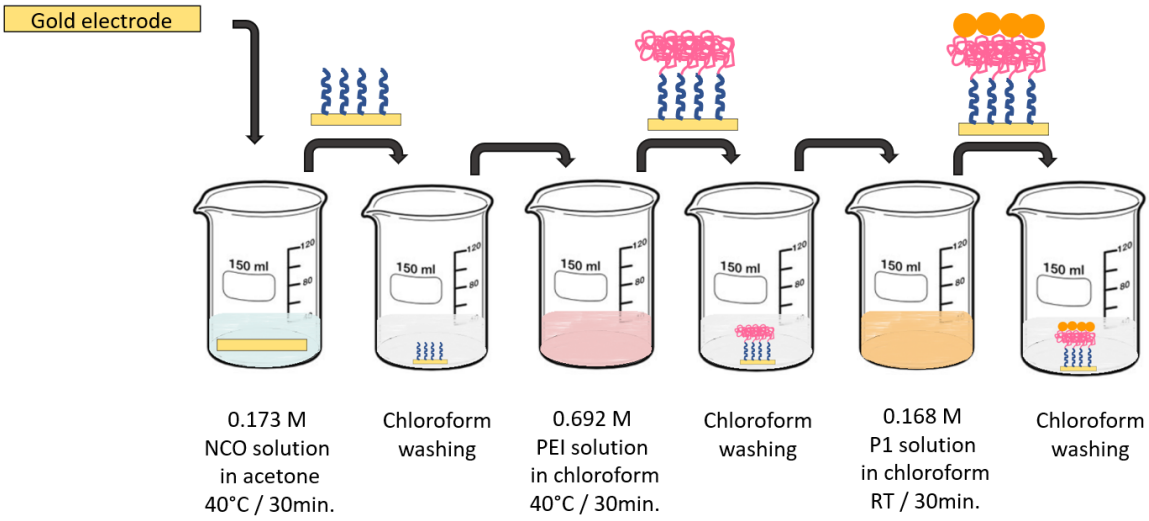

Figure 8. The process of coating gold surface by nanogel.

2.4. Constitution of Lithium-ion Conductive to Gel

2.4.1. Lithium-ion Conductive Gelation with Branched Polyethyleneimine

Polymeric gels constituted from polymer gelators. The polyester scaffold (P1), which has electron-deficient triple bonds, was used as the main substance in the gelation procedure. The branched polyethyleneimine (BPEI) was used as a secondary amine source to give a gel via Aza-Michael addition reaction with the polyester. Figure 9 shows the reaction mechanism of the addition reaction of the BPEI and the polyester scaffold which yields a polymeric gel. The chloroform was used as an organic solvent and gelling medium due to the high solubilities of the polymer gelators. The average gelling time was three minutes at room temperature with gentle stirring and without using a catalyst. The mixing gently by hand was more efficient and protect collectivity and dense of the gel against other mixing methods such as vortex or thermo-shaker.

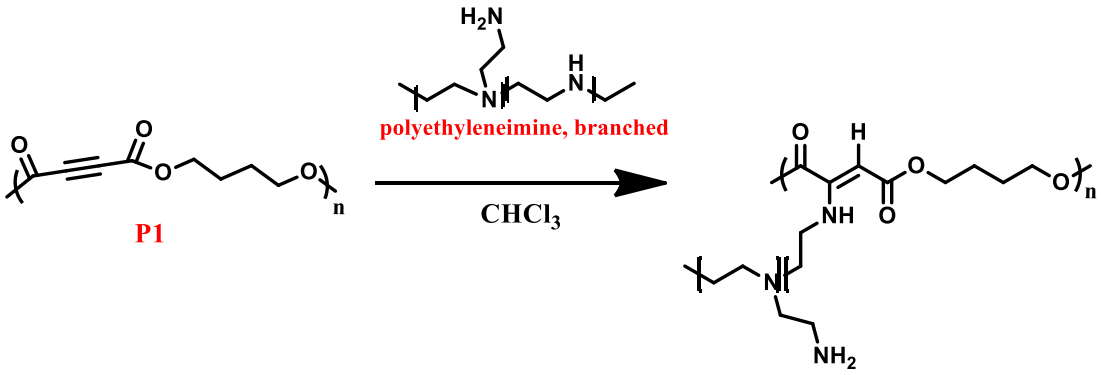

Figure 9. Reaction mechanism of the P1 polymer and branched PEI.

The 0.2 molarity of P1 polymer stock solution in chloroform was prepared as described in the literature.[61] The variable mass of BPEI in 0.1 ml of the P1 stock solution was used to achieve the gelation with the slight amine source. The number of trials and their amount of BPEI in 0.1ml (0.2M) P1 stock solution as shown in Table 1.

Table 1. The number of trials and their amount of BPEI in 0.1ml (0.2M) P1 stock solution.

Trial number	1	2	3	4	5	6	7	8	9	10
Amount of BPEI (mg)	0.11	0.12	0.33	0.36	0.40	0.45	0.5	0.55	0.56	0.66

The portion of the appropriate BPEI was determined by the decrease in the amount of liquid and the increase in the volume of gel. For this reason, the range of the appropriate substance portion was determined and trial 7 was found to be the most suitable. Thus, the bulk gel generation rates were determined by trial 7. Considering the difficulty of working with a small amount of substance, 2.32 M BPEI stock solution was prepared and 20/1 (P1 / BPEI) was added to the P1 stock solution by volume.

Then the Lithium perchlorate salt added to the polymer solution during the gelation step of the polymers. Since the lithium perchlorate was not dissolved in chloroform, ethanol was used as a solvent of salt. The maximum solubility of lithium perchlorate salt in ethanol is 151.8 g salt/100 g solvent. The maximum solubility of lithium salt in ethanol was achieved as 4.7M lithium salt in 0.04 ml ethanol at ambient conditions. Reacting with oxygen in the air, lithium forms lithium oxide (Li_2O). Therefore, it is necessary to work with the glove box where contact with air is interrupted. Since these conditions are not met, their resolution also decreases. When the $LiClO_4$/EtOH stock solution was added to the polymer solution prepared in chloroform, a homogeneous gel was observed. In the reaction, a 10 % (v/v) ethanol/chloroform solvent system was used.[64]

2.4.2. Lithium-ion Conductive Gelation with Ethylenediamine

The Aza-Michael addition reaction-based gelation with polyester scaffold was repeated using ethylenediamine as a secondary amine source. The ethylenediamine was preferred because it has a much lower molecular weight than branched polyethyleneimine. Therefore, it is aimed to increase the interaction and reaction efficiency between the two gelators. Moreover, ethylenediamine has secondary amine groups at both ends of the chain which makes it amine rich. Propylene carbonate (PC) was preferred as a gelation medium against chloroform because it is a common solvent

for lithium perchlorate salt and ethylenediamine. Also, propylene carbonate has a high dielectric constant, low toxicity and it was not regulated as a volatile. According to these features, propylene carbonate was a proper gel medium due to procures good solvent retention and high lithium-ion conductivity.

The P1 polymer dissolved in PC. The solvation procedure was carried out at 30 °C for 5 minutes. Therefore, ethylenediamine was used and the gelling procedure. This result can be obtained from the amount of gel formed. The yellow color from the polymer solution completely disappears from the solvent and appears in the gel is also evident. The ethylenediamine was dissolved (20 % (v/v)) in PC and so P1 polymer gelated via ethylenediamine in PC. The ethylenediamine was gently resinified while on the PC. Hydroxyurethane formation could be in the presence of PC and ethylenediamine. Therefore, preferably the prepared solution should be used immediately. Then, the result of the gelation was observed as agglomerated and macro-sized particles rather than small particles. Then, 0.05 M $LiClO_4$ salt solved in PC and be incorporated into the P1 stock solution before the gelation procedure.

P1 polymer (2.77 % w/v) and 0.5M $LiClO_4$ salt solution prepared in PC. Then gelling was attempted by adding different amounts of NH2 source (ethylenediamine). NH2 source was added at a ratio of 10:1 each time. Ethylenediamine prepared and used as a stock solution. The following table shows the stock solutions and ethylenediamine ratios in gelation. (Table 2).

Table 2. Ethylenediamine stock solution ratios and specimen codes that used.

ethylenediamine amine stock in 200µl PC (µl)	ethylenediamine %
10	0.4
15	0.6
20	0.8
25	1
30	1.2
35	1.4
40	1.6
45	1.8
50	2
55	2.2

Dissolving salt in a solvent increase the electrolyte conductivity as a function of salt concentration (by increasing the number of charge carriers). Further increase in Li^+ concentration may result in lower ionic mobility by recombination of ions to neutral contact ion pairs. Therefore, high salt concentration does not always result in high conductivity. However, the conductivity of any aprotic Li-salt based electrolyte depends not only on the salt concentration but also on the anion, solvent composition, and temperature. Therefore, the highest conductivity can be achieved even at low concentrations using the PC / EC solvent system.[65-67] The electrolyte gel was composed of mixed solvent as a function of EC/PC molar ratio 1 at 0.5molar LiClO4 with polyester scaffold and ethylenediamine. The solvent molar ratios determined from the literature.[68]

2.5. Characterization Techniques

2.5.1. Electronic Characterization

Multimeters is an electronic measuring instrument that combines many different measuring techniques such as voltage, current, and resistance. They are highly preferred because they are portable (bench-top) and give fast results. Resistivity measurements of gels were performed with HP 34401A multimeter by placing gel between two ITO's and specially designed PMMA blocks. We performed the measurements as resistance to the current-dependent current transition. The electrical conductivity calculation was done as shown in equations 2.1 and 2.2. Where L is the length of the conductor measured in meters (m), A is the cross-sectional area of the conductor measured in square meters (m^2), ρ is resistivity, and σ (sigma) is the electrical conductivity measured in siemens per meter ($S \cdot m^{-1}$).

$$\rho = \frac{R \times A}{L} \tag{2.1}$$

$$\sigma = \frac{1}{\rho} \tag{2.2}$$

Resistivity measurements of gels were taken between two ITO's and compressibility was kept constant as 2 millimeters by specially designed PMMA blocks, as shown in Figure 10. So, calculation of conductivity was calculated accurately, and solvent evaporation prevented.

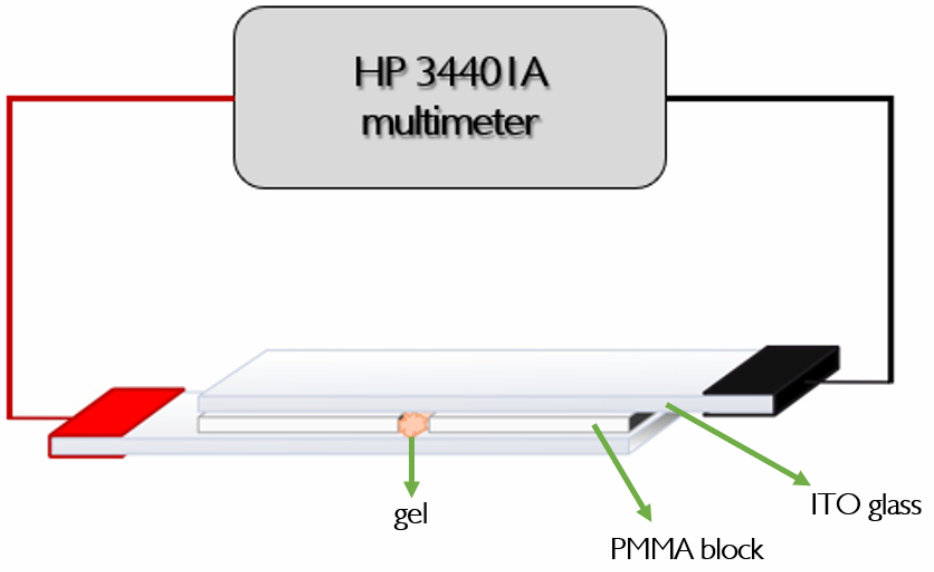

Figure 10. General representation of resistivity measurement setup.

2.5.2. Electrochemical Characterization

Electrochemistry is a branch of chemistry that deals with the reactions that take place at an interface with an electronic conductor (metal, graphite, or semiconductor) and an ionic conductor (electrolyte). The potential, current, and charge is a basic electrochemical signal which acts as an analytical signal. Hence, by way of measuring electrochemical signals, we can easily determine the analyte concentration and its chemical reactivity.[69] Also, electrochemical characterization techniques are appropriate for nano/micro materials. Electrochemical characterization is the most powerful technique for energy storage devices; such as batteries, capacitors, and also for sensor systems because it involves interface reactions. [70-73]

The three-electrode system is much preferred to specially study the behavior of the analyte at the interface of the electrode. Electrochemical characterization of three-electrode systems consists of an electrochemical cell, electrolyte solution (material), a reference electrode, a counter (auxiliary) electrode, and a working electrode. The reference electrode has a stable potential in time while the working electrode's potential is varying with time and usually made of silver/silver chloride (Ag / AgCl) or saturated calomel (SCE). Also, the electrochemical reaction takes place on the working electrode. The counter electrode allows passing current from the signal source to the working electrode. The purpose of the electrolyte is to provide ion during the redox reaction. [74]

Cyclic voltammetry (CV) and electrochemical impedance spectroscopy (EIS) experiments were performed using a Gamry REF600 potentiostat/galvanostat. As working electrodes, nanogel functionalized gold surfaces were used. All electrode potentials cited in this work were measured against Ag/AgCl (saturated KCl) and the counter electrode was a platinum wire at room temperature. As an electrolyte solution, 0.01 M phosphate buffer with 1 mM $K_4Fe(CN)_6$ solution was used. Before the measurements, aqueous solutions were deoxygenated by bubbling nitrogen. Impedance spectra in the range 10^5-10^{-1} Hz were recorded with 10 mV/rms amplitude potential perturbation.

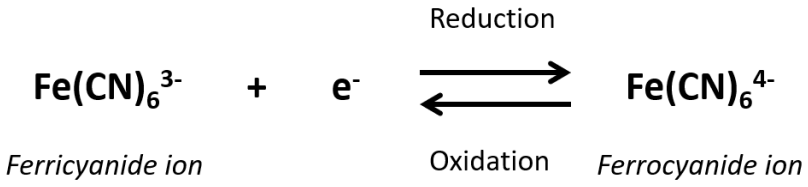

Figure 11. In this one-electron redox reaction, the ferricyanide ion $[Fe(CN)_6]^{3-}$ is an oxidant and the ferrocyanide ion $[Fe(CN)_6]^{4-}$ is a reductant.

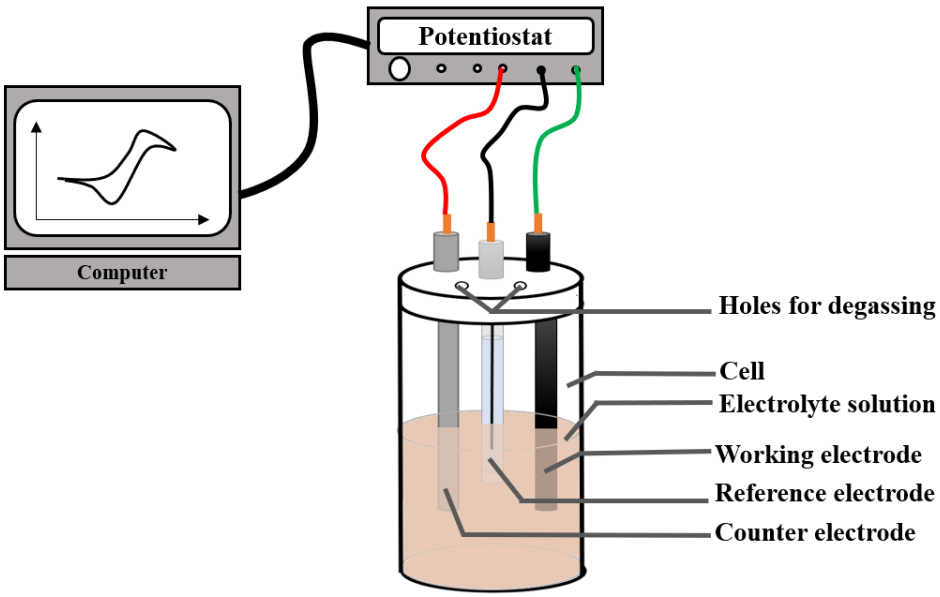

Figure 12. Schematic representation of a three-electrode electrochemical cell system.

2.5.2.1. Cyclic Voltammetry

In the voltammetric techniques, varying potential is applied to an electrochemical cell concerning time, and current is measured as a function of applied potential which called a voltammogram. In cyclic voltammetry, the potential is applied by sweeping between the chosen limits at a constant rate called the sweep rate or scan rate. The cyclic voltammogram gives the oxidation/reduction (redox) peaks of the analyte and used in studying electro activity properties of compounds.[75]

The two important parameters of the cyclic voltammogram are the peak potentials of the anodic and cathodic peaks and their peak currents. If the electron transfer at the working electrode surface is faster than other processes such as diffusion, the reaction is reversible and the difference between the anodic and cathodic peak potentials, which called peak-to-peak separation will be high. The difference between oxidation and reduction potentials is called half-wave potential ($E_{1/2}$). This potential gives information about how easily the donor oxidizes. A donor gives information about how easily oxidized it will be a candidate for good conductivity. Also, the potential scanning window, direction, and scan rate are determined by the reducing/oxidizing species.

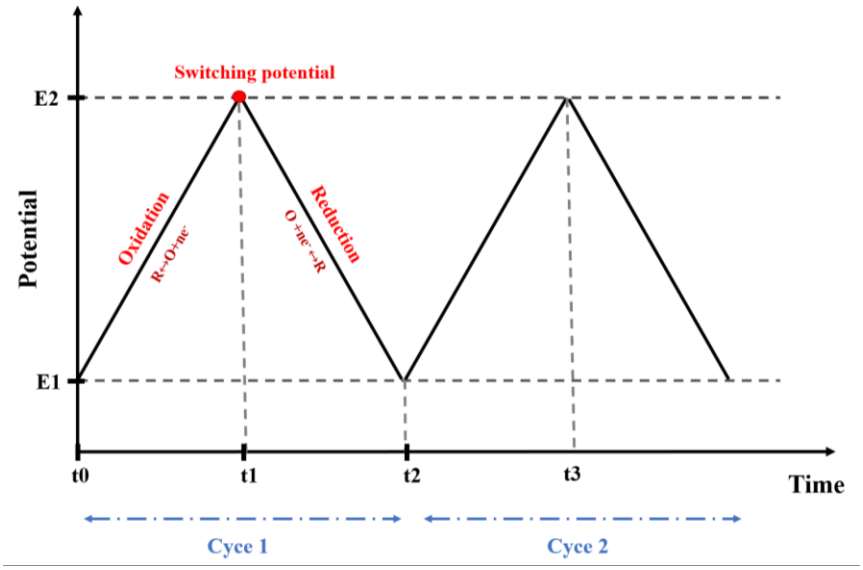

Figure 13. Example of a triangular potential waveform applied in the generation of a cyclic voltammogram.

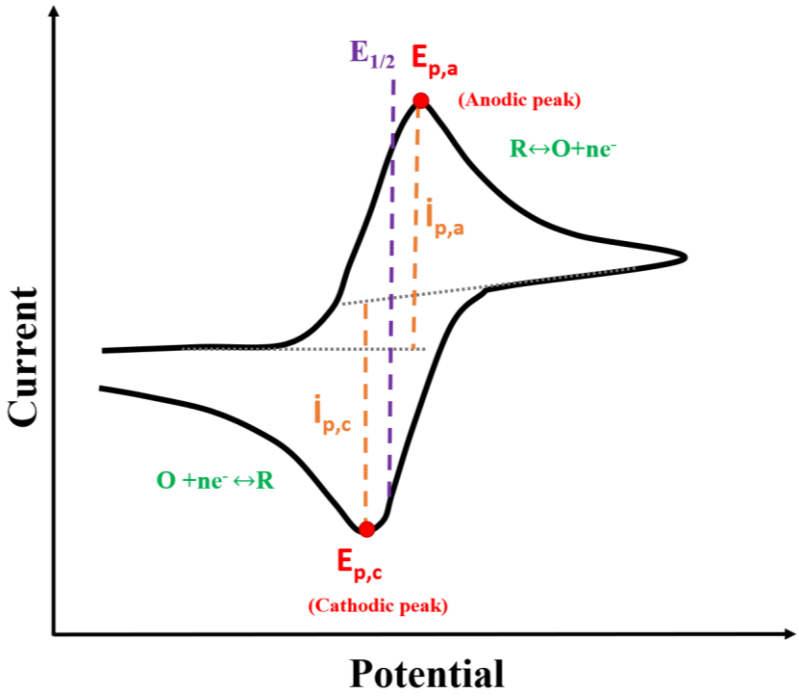

Figure 14. The cyclic voltammogram of single e^- showing the measurement of the peak currents and peak potentials.

2.5.2.2. Electrochemical Impedance Spectroscopy

Impedance is a measure of the resistance to the flow of an alternating current (AC) and it is a non-destructive technique. Alternative voltage, which is a function of the electrochemical impedance frequency, can be applied to these voltage values as an alternating current (AC) response of a circuit. When the direct current (DC) is applied, the current is measured, and the resistance is defined by Ohm's Law.

$$E = I\,R \tag{2.3}$$

If alternating current is applied, the frequency value is not zero. In this case, the equation is changed like this:

$$E = I\,Z \tag{2.4}$$

Here, Z represents the resistance in the AC circuit. The AC stimulation signal is expressed as a function of time and is given by the correlation below.

$$E_t = E_0 \sin(\omega t) \tag{2.5}$$

The potential at the moment of t is E_t, E_0 is the amplitude (magnitude) of the signal, and ω is the angular frequency. The relation between angular frequency (ω, radians/second) and frequency (f, Hz) is as follows.

$$\omega = 2\pi f \tag{2.6}$$

The response of the current to an oscillating input potential. The current response that corresponds to Equation 2.4 has the same frequency but shifted in the θ phase. (Figure 15)

$$I_t = I_0 \sin(\omega t + \theta) \tag{2.7}$$

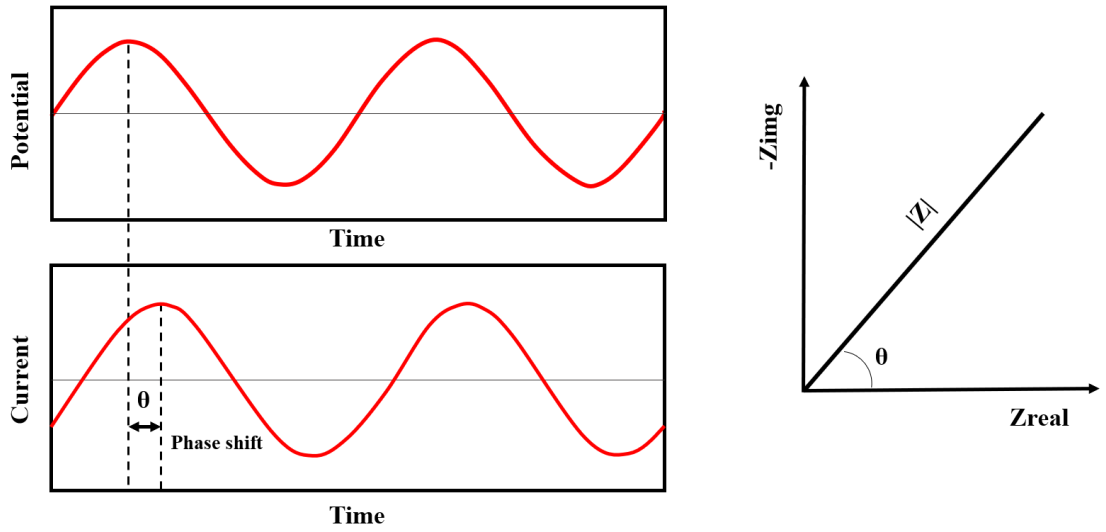

Figure 15. Illustration of voltage input and current output showing amplitude difference and phase shift.

The impedance can be obtained by dividing the potential-time function by the current-time function. It is also possible to achieve Impedance as a complex function using Euler's equation.[75]

$$\exp(j\theta) = \cos\theta + j\sin\theta \tag{2.8}$$

$$E_t = E_0\sin(j\omega t) \tag{2.9}$$

$$I_t = I_0\sin(j\omega t+\theta) \tag{2.10}$$

$$Z(\omega) = E/I = Z_0\exp(j\theta) = Z_0(\cos\theta + j\sin\theta) \tag{2.11}$$

$$Z(\omega) = Z' + jZ'' \tag{2.12}$$

In addition to the resistor, the capacitor and inductor also prevent electron flow. The table summarizes the response to the oscillating input, impedance for three common circuit elements.[75]

Table 3. The impedance of common circuit elements.

Component		Impedance
Resistor	R	R
Capacitor	C	$1/j\omega C$
Inductor	L	$j\omega L$
Warburg	W	$1/T\ (j\omega)$
Constant phase element	CPE	$1/T(j\omega)^a$

The frequency-dependent impedance spectrum of an electrochemical system is usually shown on the Nyquist and Bode curves. The Nyquist curve is the curve in which the real and imaginary components of the impedance data assigned for each frequency value are displayed throughout the frequency range in which EIS analysis is performed. Each point in the Nyquist graph corresponds to the impedance value at a fixed frequency. [75-77]

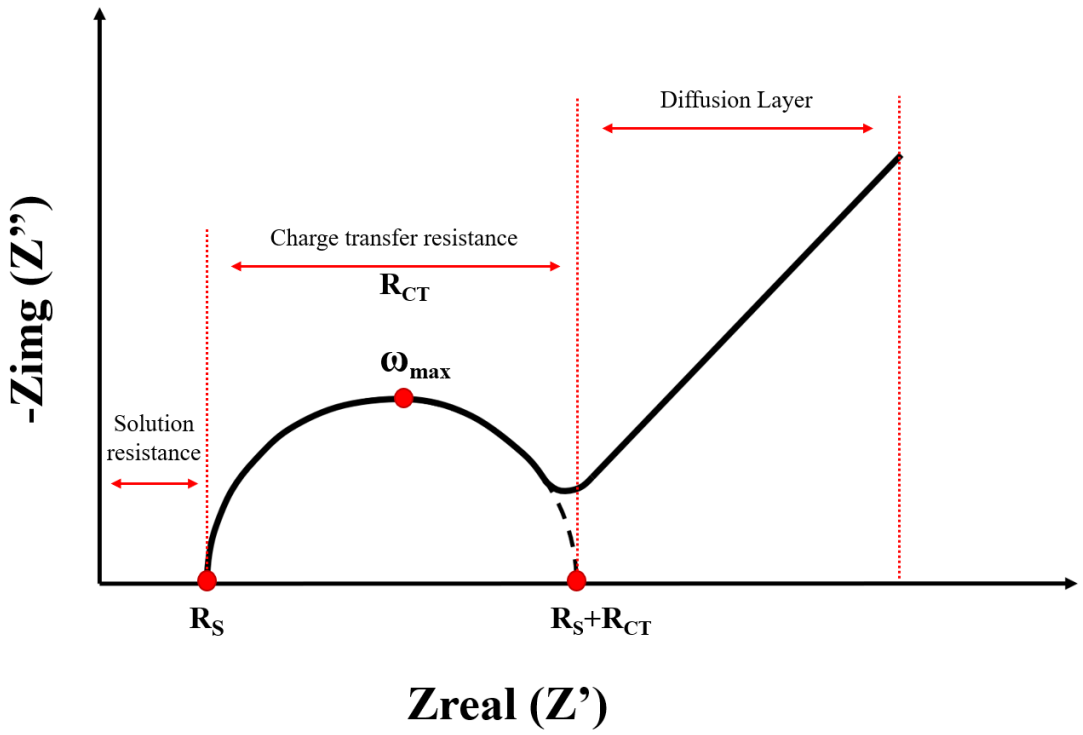

Figure 16. Schematic of typical Nyquist plot.

EIS spectra fitted to Randles circuit which was consist of constant phase element (CPE), parallel connected charge transfer resistance (Rct), and series-connected open Warburg element (Wo); all in series with the active electrolyte resistance (Rsol). The incomplete semi-circle in the Nyquist plot was corresponding to capacitive behavior. The capacitance from constant phase element and resistance of charge transfer was calculated;

$$C = R \wedge (1-n/n) * Q \wedge (1/n) \quad (2.13)$$

2.5.3. Fourier Transform Infrared (FTIR) Spectroscopy

Infrared spectroscopy deals with the infrared region of the electromagnetic spectrum (wavelength from 700 nm to 1 mm) and it is based on the vibrations of the atoms of a molecule of interest. The infrared spectrum is generally subdivided into three regions which are near-IR, mid-IR, and far-IR as shown in Table 4. [78] IR spectrum represents either the infrared radiation which is absorbed or transmitted by the sample. Because each different material is a unique combination of atoms, two compounds cannot produce the same infrared spectrum. That is why infrared spectrometry provides an identification which is called qualitative analysis.

Table 4. Infrared spectral regions

Region	**Wavelengths, μm**	**Wavenumbers, cm $^{-1}$**
Near	0.78 to 2.5	12800 to 4000
Middle	2.5 to 50	4000 to 200
Far	50 to 1000	200 to 10

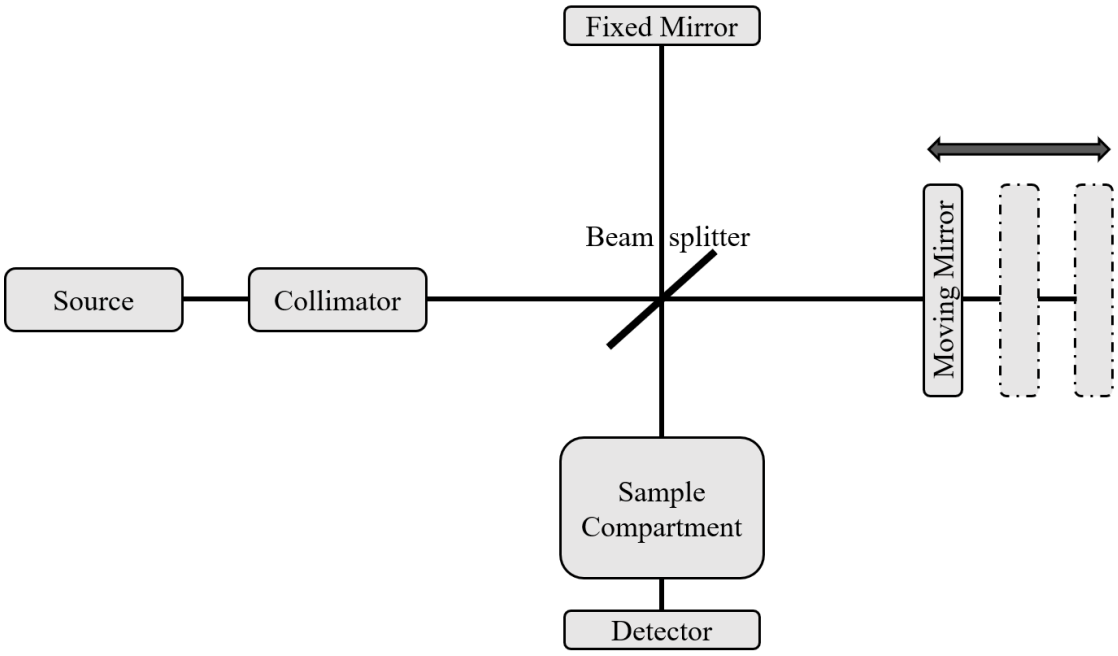

Figure 17. A general Fourier Transform Infrared (FT-IR) spectrometer block diagram.

2.5.3.1. Attenuated Total Reflection (ATR)

The main difference between reflection and transmission FT-IR techniques is the challenging sample preparation of transmission FT-IR even though transmission FT-IR techniques are convenient for solids, liquids, and gases. Reflection FT-IR techniques, however, require minimal sample preparation and can be used to analysis of not only solids and liquids, but also gels or coatings.[78]

Classical FT-IR techniques such as transmission or ATR techniques generally measuring coatings or samples on samples where the thickness of the sample. Therefore, the infrared beam passes through a much longer path through the sample than with small angles and creates a stronger spectrum Infrared measurements were carried out using PerkinElmer Spectrum 100 FT-IR with an attenuated total reflection apparatus in a spectral range between 600 and 4000 cm^{-1} to observe functional groups of gels. A schematic representation of the beam path of the reflectance of ATR device is shown in Figure 18.

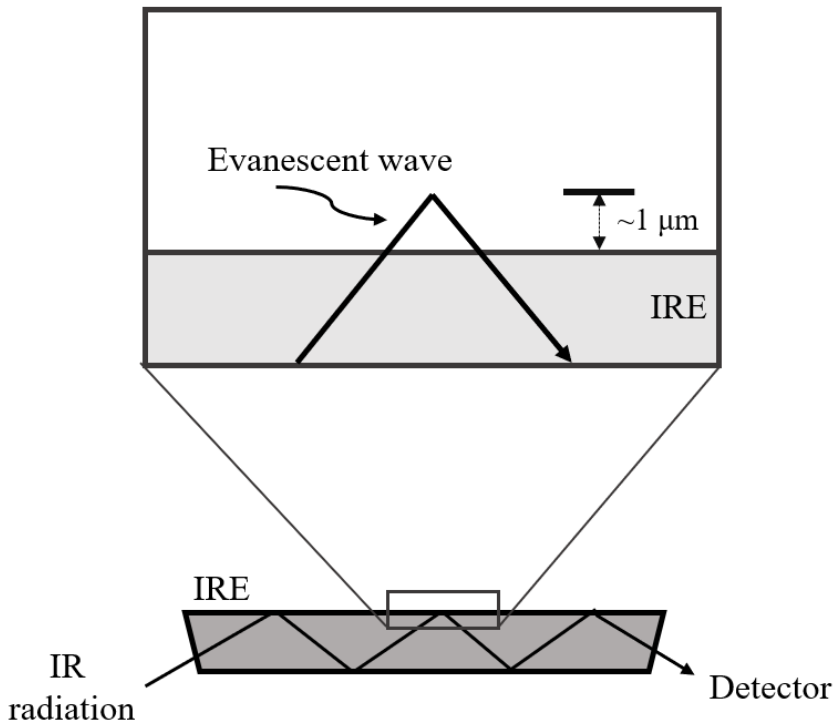

Figure 18. The general working principle of attenuated reflectance ATR device.

2.5.4. Atomic Force Microscopy

Atomic force microscope (AFM) is a very high-resolution scanning force microscope. The achieved resolution is higher than optical techniques. The AFM consists of a flexible lever and a pointed tip (used to scan the surface). A tip with a radius of curvature on the nanometer scale carries. When the tip is brought to a distance close to the sample surface, forces between the tip and the surface cause the Hooke law to bend the lever. Depending on the situation, the forces measured in the AFM can be mechanical contact force, van der Waals force, capillary force, chemical bond, electrostatic force, magnetic force, etc. Along with the forces, other features can be measured simultaneously with special type sensing techniques. Usually, the bend in the lever is measured by a laser beam projected from one end of the lever to the detector (a series of photodiodes). Figure 19.

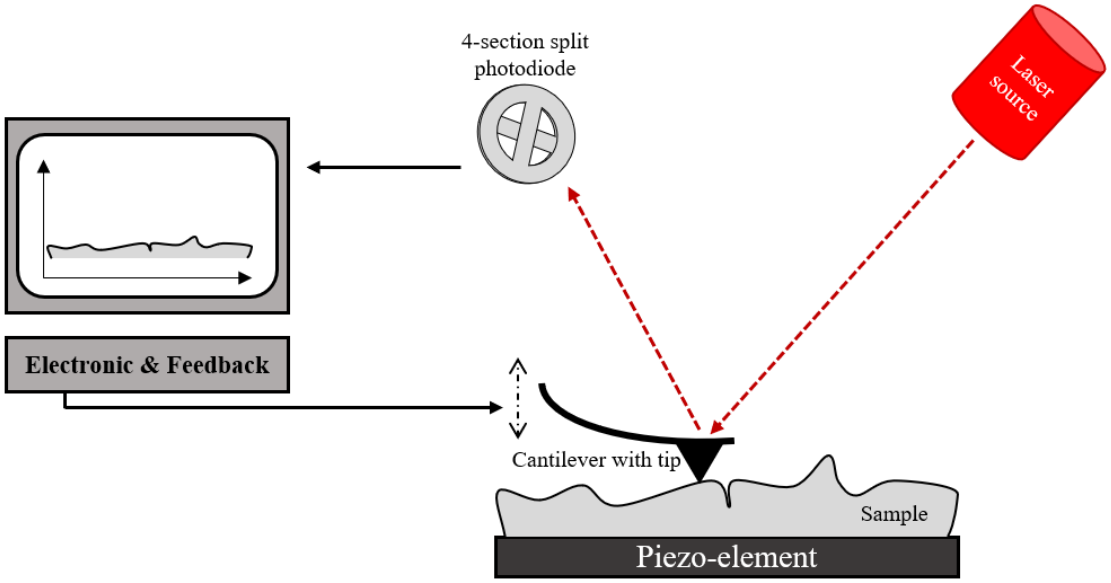

Figure 19. General representation and working principle of the AFM device.

2.5.4.1. Electrostatic Force Microscopy

Electrostatic force microscopy (EFM) is a type of dynamic non-contact atomic force microscopy where the electrostatic force is probed. ("Dynamic" here means that the cantilever is oscillating and does not contact the sample). This force arises due to the attraction or repulsion of separated charges. It is a long-range force and can be detected 100 nm or more from the sample.[79]

2.5.6. Nuclear Magnetic Resonance (NMR) Analysis

1-H NMR spectrum was recorded in the solution of CDCl3 on Varian 400 spectrometers for Fc-BPEI characterization.

CHAPTER 3

RESULTS & DISCUSSIONS

3.1. Characterization of Electroactive nanogel on the gold surface

The bulk sample was prepared with polyester and branched polyethyleneimine in chloroform medium as previously explained in detail. The polymeric nanogel was prepared by layer by layer grafting of polyester (P1) and branched polyethyleneimine (BPEI) on the gold surface. Figure 20.

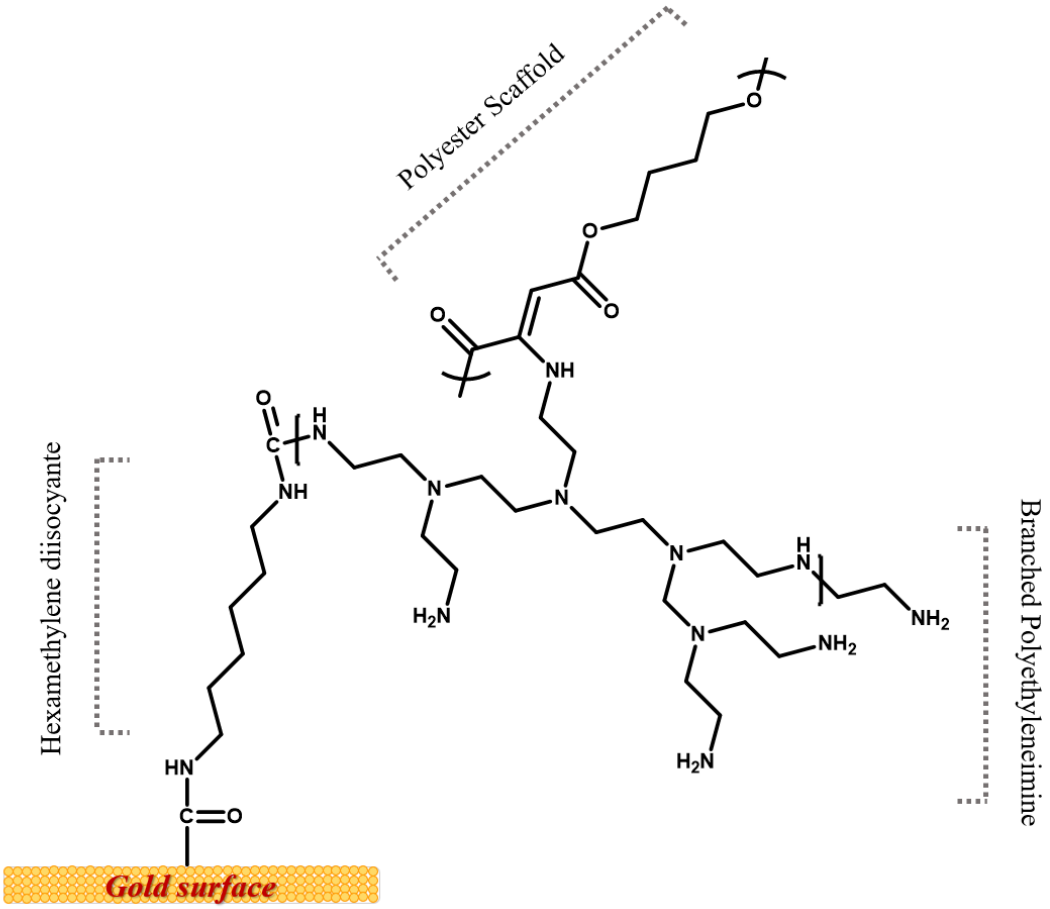

Figure 20.Schematic representation of 3step nanogel grafted on gold surface.

The P1 polymer, bulk gel, 3 and 9 steps nanogel grafted gold surfaces characterized by ATR-FTIR spectroscopy. The FTIR spectrum is shown in Figure 21. The strong band at 1715 cm^{-1} refers to the ester carbonyl (C=O) stretching. The band due to the C-O-C asymmetric stretching vibration of ester occurs at 1233 cm^{-1} and symmetric stretching vibration occurs at 1040 cm^{-1}.[80, 81] These stretching vibrations arising from esters strongly determined both P1 polymer and at all the gel samples. The C-H stretching vibrations occurs at 2854 cm^{-1}, 2922 cm^{-1}, 2957 cm^{-1} and C-H bending at 1460 cm^{-1}.[80] The signal at 1573 cm^{-1} corresponds to C=C conjugated with C=O coupled with N-H bending vibration of amines. The signal at 1145 cm^{-1} is responsible for the C-N stretching of amines.[81, 82] Although, the weak amine N-H stretching vibrations not observed, N-H bending and C-N stretching vibrations proofed the BPEI existence.

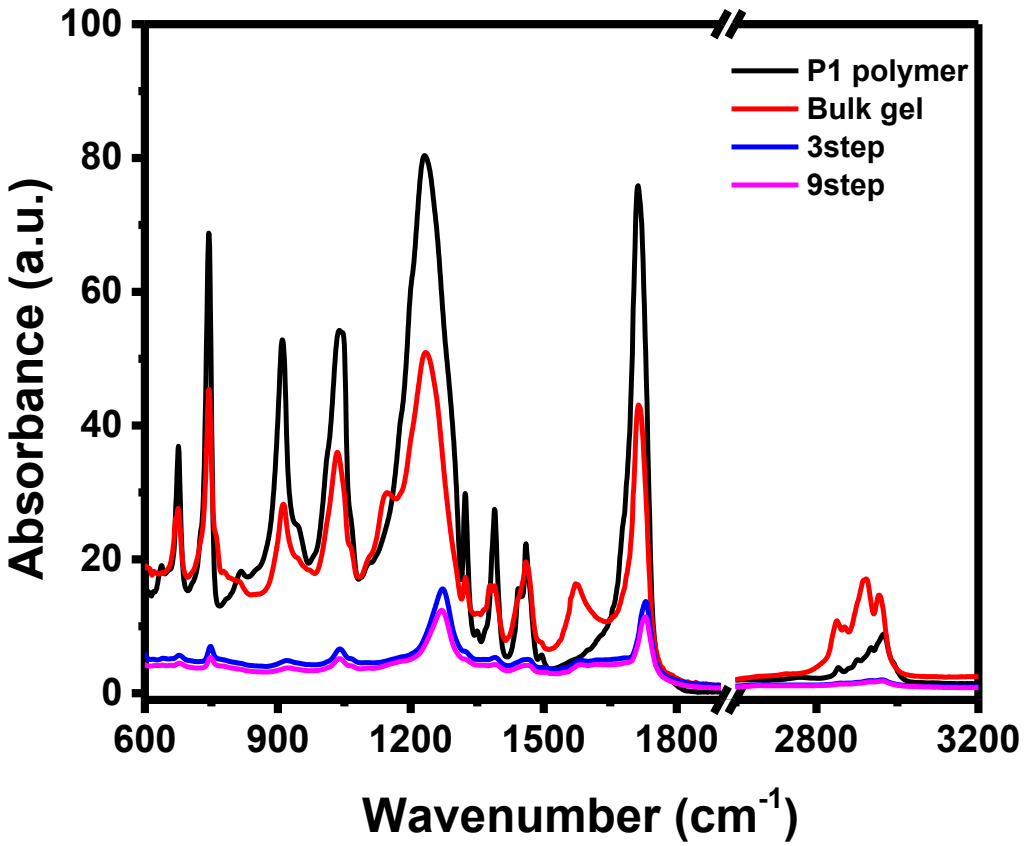

Figure 21. The FT-IR spectrum of P1 polymer, bulk gel, and nanogels in different heights.

The gold surface was modified by layer-by-layer reactive coating of polyester (P1) / polyethyleneimine (BPEI) based gel. The nanometric gel (nanogel) coated surfaces

entitled as the number of steps that coated on the gold surface. For all samples, the first step is grafting isocyanate group on the gold surface. The post-functionalization done at this step. Then, BPEI and P1 coating is done, respectively. The minimum number of coatings is 3, and the maximum number of coatings is 9. Reactions are always terminated with the BPEI polymer.

The nanogel coated gold surfaces topographical properties were examined by Atomic Force Microscopy (AFM). According to AFM images, it is proved that the entire gold surface is effectively covered with gel. Figure 22 shows the AFM topography images and cross-sections of 3step, 5step, 7step and 9step polymers grafted or coated gold surfaces. Each topography image shows 40μm² area of the surface. The general particle distributions and height differences observed by the AFM topography images. The 3step polymer grafted gold surface, Figure 22/a there is a non-homogeneous distribution and aggregates observed compared to other examples. Figure 22/b has the lowest overall height difference with 100nm, compared to others. The height/distance, cross-sections of the topography images were taken from the arrowed line. The line drawn to show general characteristics of the surfaces. For instance, while the layers or steps of the coated polymers increased, the height difference of the cross-section is balanced, and number of the aggregates decreased. In addition, the maximum height differences of the 3step and 9 step surfaces is almost same, 200nm, while their variation in the roughness is distinct. Other examples where the height difference is less are 7step and 3step, respectively. From height differences variation of negative and positive scale also shows the roughness characteristics.

The quantitative roughness analysis done with AFM. Table 5 shows the 40μm² area roughness and line roughness of the Figure 22. The line roughness was taken from the arrowed line that also used for cross-section. The entire gold surface can be covered with gel, with a minimum of 3 step reactions. Therefore, the surface roughness is important in determining the most effective and homogeneous surface coating layer number. The 3step, 5step, 7step and 9step samples area roughness are 231.05nm, 300.28nm, 360.08nm and 377.9nm, respectively. The area roughness of the samples is gradually increased in direct proportion of the number of the polymer steps/layers that coated. Thus, there is an effective layer-by-layer coating on the surface. The increase in roughness is related to the aggregate-dependent coating passes into irregular form due to the strong interaction between layers. The line roughness measurements were made from

the line drawn across the surface to reflect the overall characteristics of the surface. The line roughness values change independently from the number of coating layers that gives an information about the surface homogeneity. The 5step polymer grafted gel sample has the lowest and finest roughness than others.

Table 5. Shows area roughness and line roughness of each step in Figure 22.

Sample	Area Roughness (nm)	Line Roughness (nm)
3step	231.53	153.05
5step	300.28	47.56
7step	360.08	103.3
9step	377.9	182.24

The 5step gel coated gold surface produced by a layer by layer polymer coating. The reproducibility was examined by repeating the 5step gel coated gold surface without changing conditions. Each sample prepared on different days. Their topography characteristics examined by AFM. Table 6 shows 3 different 5step gel coated surface and their 40micrometer square area roughness. All samples area roughness is approximately 300 nm and show the same characteristic. However, gels adhesive property causes local aggregates. As a result, we can say that the gel coated gold surface has a reproducibility.

Table 6. AFM area roughness of the samples in Figure 23.

Sample	Area Roughness (nm)
a	315
b	275.56
c	300.28

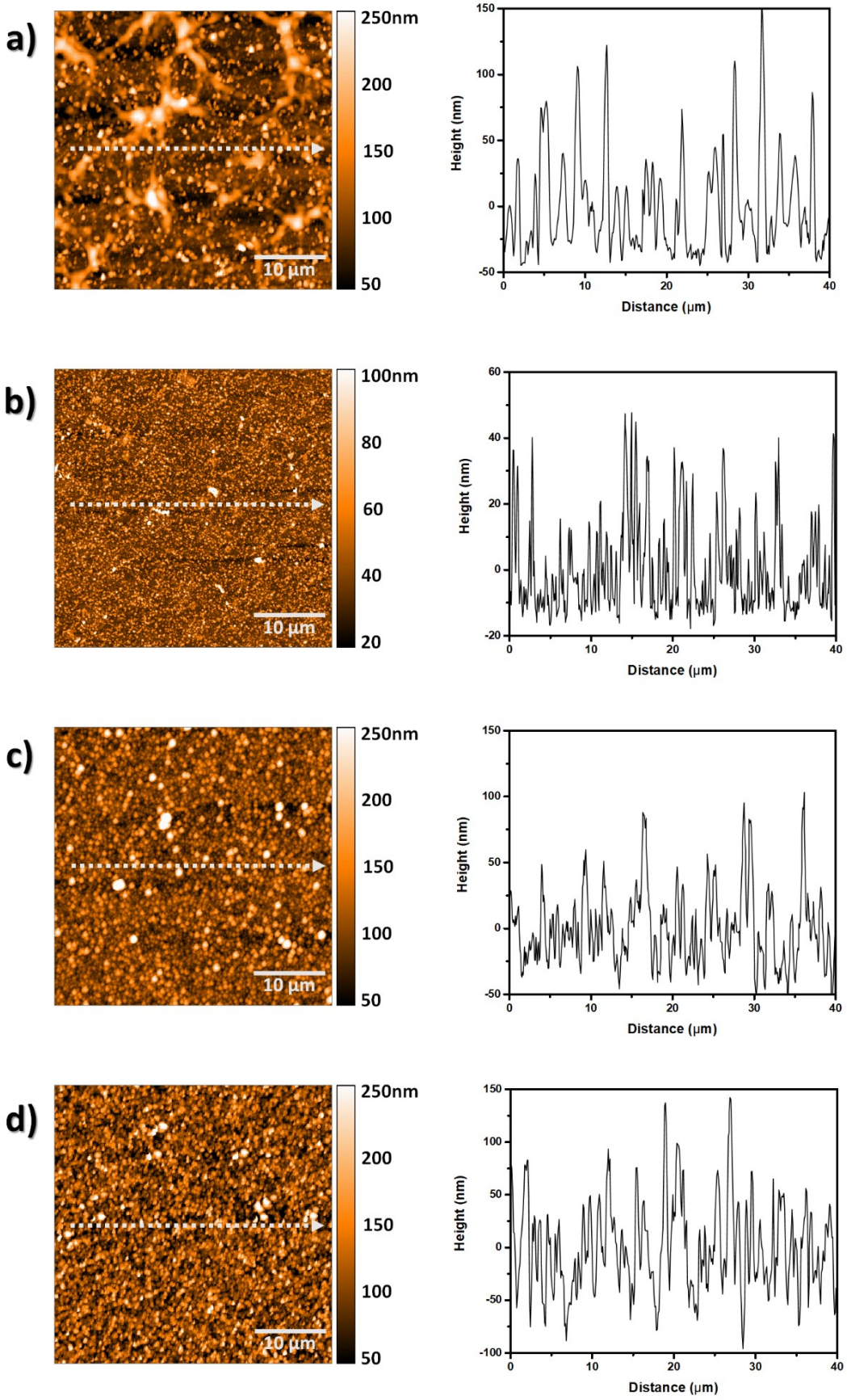

Figure 22. AFM topography images and their dashed line cross-sections. a)3step, b)5step, c)7step, d)9step.

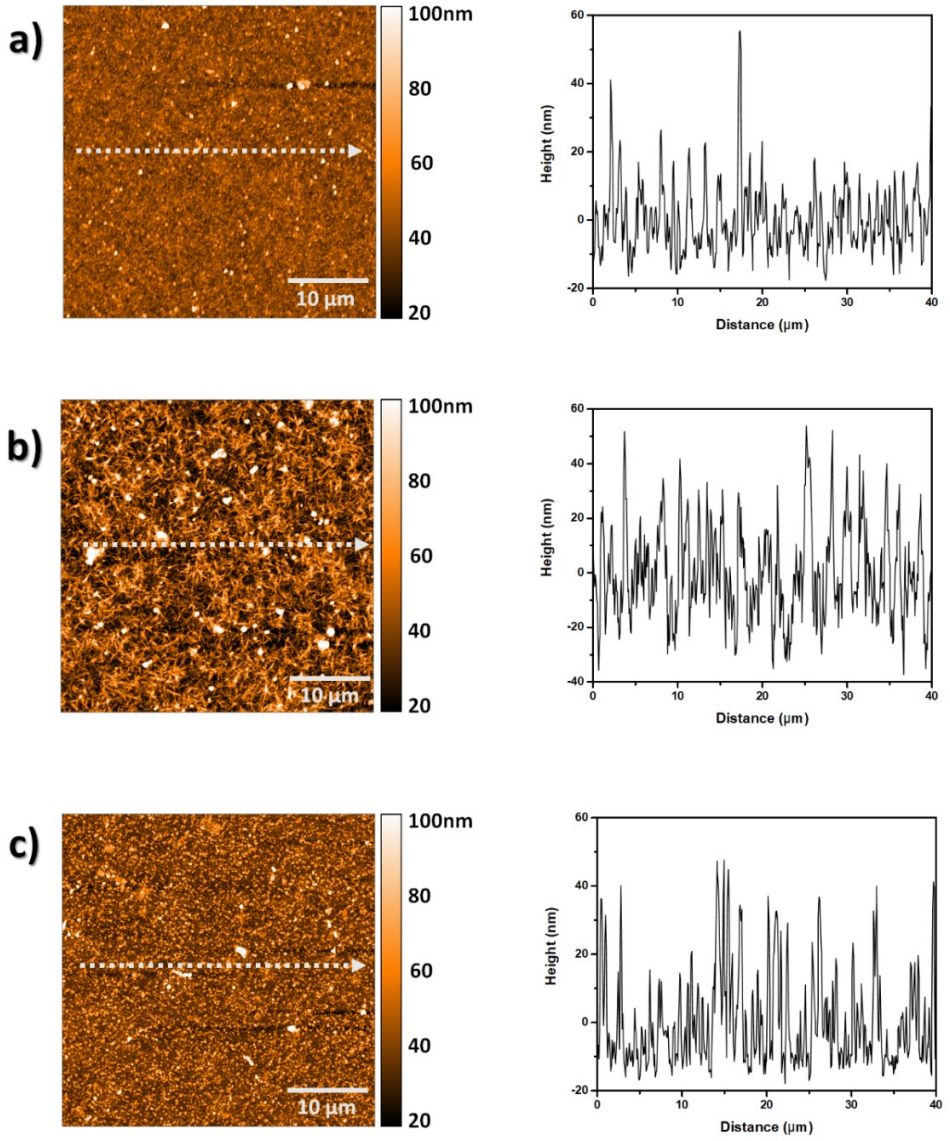

Figure 23. 5step gel coated gold AFM topography images and their dashed line cross-sections, respectively.

The AFM image of the nanogel obtained because of 6-step after being pacified with 11-Mercapto-1-undecanol to determine thickness via AFM. (Figure 24) As seen in the AFM image, the nanogel consist of tightly stacked globular homogeneous polymer domain on the gold surface. The cross-section line one and two show identical elevation with an average height of 400 nm in Figure 25 c and d. The 25 µm² area roughness result of gold and polymer region is nearly 40 nm and 600 nm respectively which can be interpreted as a result of the porous nanogel structure. These results indicate that the three-dimensional nanogel structure formed because of high-efficiency polymer grafting on the gold surface.

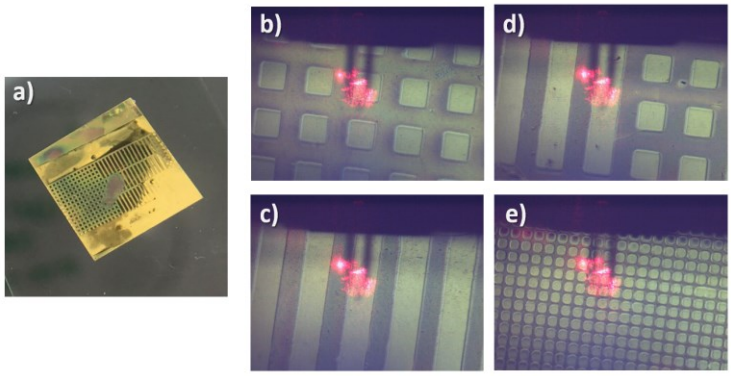

Figure 24. 6 step polymer grafted gold surface images, with PDMS stamp. b, c, d and e were taken via AFM camera.

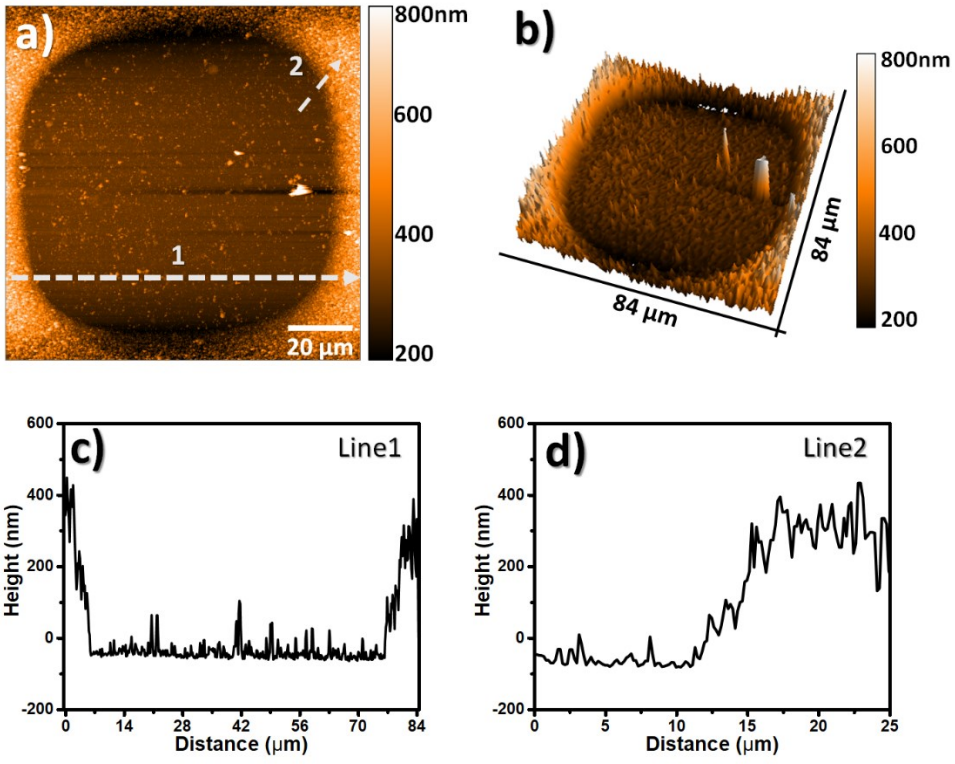

Figure 25. The 6-steps polymer grafted gold surface, (the square region was passivized with 11-Mercapto-1-undecanol) a) AFM topography image (ElectriMulti-75G), b) 3D chart view of figure c, d) cross-section of white dashed line 1 and 2 respectively.

Then EFM measurements done with 2cycle 6-steps polymer grafted gold surface which specific areas passivated by SH. In order to find the appropriate voltage range to be applied during the measurement, tip voltage, IV curve between -4 / + 4 V was obtained from passivated (red) and polymer coated (black) points. -3V / + 3V, which is the highest phase interval, was chosen in response to the applied potential of the gold and polymer coated areas. (Figure 26)

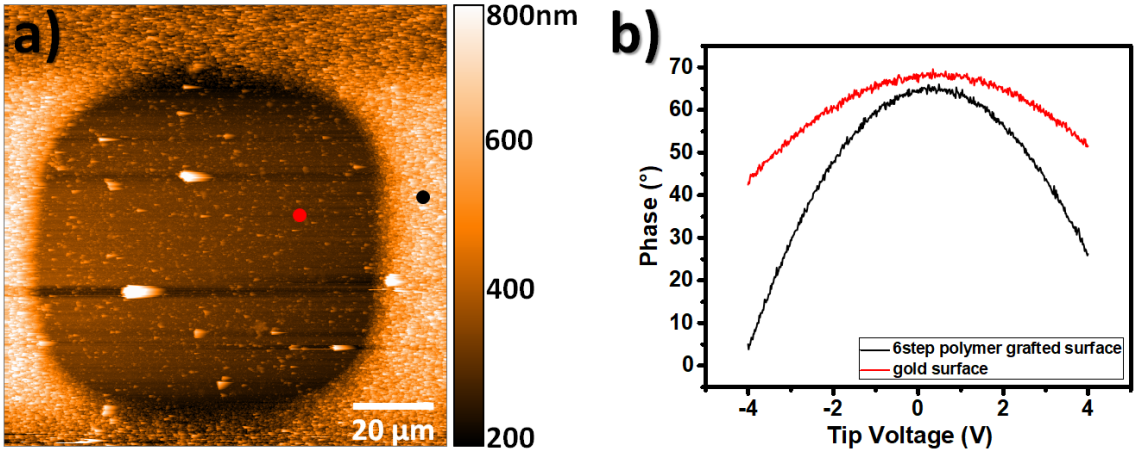

Figure 26. a) IV curve between -4 / + 4 V was obtained from passivated (red) and polymer coated (black) points and b) Phase vs tip voltage curves of gold surface and polymer film.

EFM was used to determine the stored charge and local electrostatic properties stored by using the polarity of nanogel surfaces at atmospheric pressure. Considering the differentiation of phase to the tip voltage graph of the nanogel and gold surface, the tip voltage was chosen as ±3 volts (Figure 27), and the tip voltage 0 V was carried out for reference EFM measurement. All EFM measurement was conducted double-pass mode with 40 nm second tip lift. Figure 27 a, b and c show the phase image obtained when -3, 0, and +3 volts are applied to the tip, respectively. There is a contrast differentiation prominently at +3 and -3 volts between the polymer and the gold layer however, the entire surface shows the identical behavior at 0 volts. According to the phase image, Figure 27 d, e and f shows the phase shift obtained when -3, 0, and +3 volts are applied to the tip, respectively. When -3 volts is applied to the tip, the phase shift is 15 degree between nanogel and gold layer, and +3 volts is applied 20 degree shift is obtained. These results

demonstrate that the +3 volts charged tip tends to interact more with the nanogel on the gold surface than the -3 volts. Also, results may indicate that +3 volts reduce the effective resonance frequency and capacitive electrostatic force become higher on the nanogel.

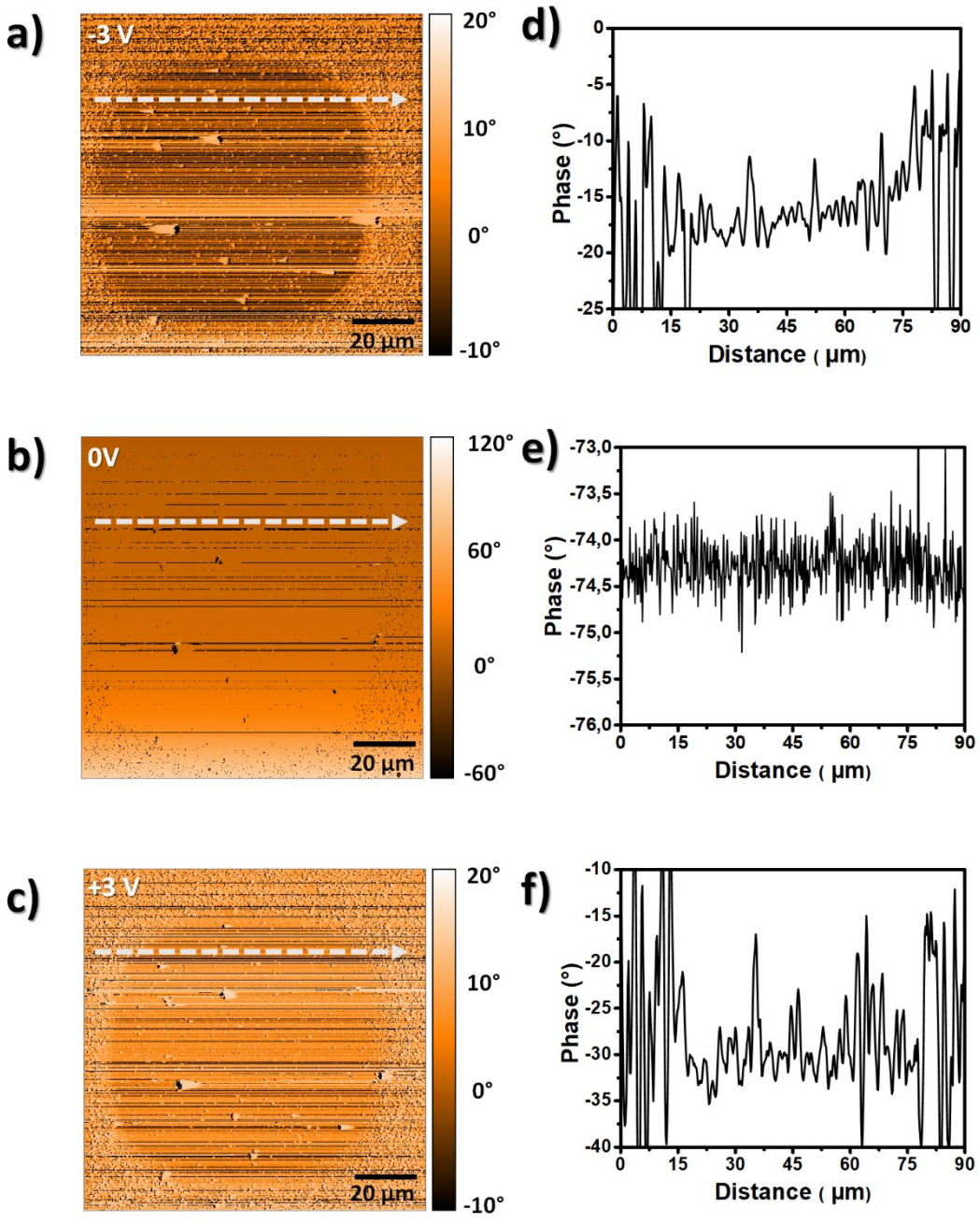

Figure 27. EFM image after 6-step nanogel form with a, b and c) respectively -3, 0, and +3 V respectively and d, e, and f their phase shift profiles. (Multi75E-G)

Figure 28 shows the Cyclic Voltammogram (CV) measurements each different step/layer of polymer coated gold surface to produce a gel. The bare gold (gold coated glass) surface CV was also taken to compare with gel coated surfaces. The 1mM potassium ferrocyanide ($K_4Fe(CN)_6$) in 0.01M phosphate (PBS) buffer used as an electrolyte solution The potential range is 0.7 / -0.3 V with a scanning speed of 50 mV.

As seen in Figure 28, the bare gold surface anodic and cathodic peak current is 73 µA and 71 µA, where the potentials are 0.38V and 0.07V. The peak current of the 3-step nanogel was gradually decreased, while the anodic and cathodic peak current sizes are 57 µA and 66 µA, respectively. The 5-step nanogel anodic and cathodic peaks are 57 µA and 71 µA. The nanogel coated surfaces has a relatively small peak current and narrow peak separation. While the steps/layers of the grafted/coated polymers are increased, the surface becomes thicker. The surface thickness directly affects the electron transfer of the soluble species and essentially blocks the ion migration. Although nanogel does not completely block electron transfer, relatively small peak currents are indicative of a slow electron transfer. However, The peak currents for 7step and 9step nanogel coated gold surface peak current are dramatically decreased and blocks the electron transfer of the $K_4Fe(CN)_6$. The CV results shows relatively the same anodic peak current, the 5-step grafted surface has slightly great cathodic peak current. Hence, the reduction of the ferricyanide is easy to take place in 5-step, compared to 3-step. Because of the 5step nanogel is more organized and apart from incorrectly orientated aggregates.

The anodic and cathodic peak potentials of 3step and 5step nanogels are 0.27V and 0.14V, respectively. A negative shift in the cathodic peak potential, and a positive shift in the potential of the anodic peak, were observed in the voltammogram of the 5-step nanogel. The reason for this behavior of nanogel is that $[Fe(CN)_6]^{3-/4-}$ ions are more difficult to reduce / oxidize than naked gold.[29]

Figure 29 shows the cyclic voltammogram of the 5step nanogel on the gold surface with multiple repetitive cycles. The anodic and cathodic peak currents and electro-generated ferricyanide ions ($[Fe(CN)_6]^{3-}$) reduction is faster that oxidation of ferrocyanide ($[Fe(CN)_6]^{4-}$) ions while the pH is 6.8. The peak currents gradually decrease because of the depletion of electroactive species at the electrode surface, while the number of the cycles are increased. There is no significant change in peak separation due to number of cycles. Also, CV scanning towards increasingly positive potentials and first oxidation signal of $[Fe(CN)_6]^{4-}$ ions are observed then produced $[Fe(CN)_6]^{3-}$ ions are reduced.

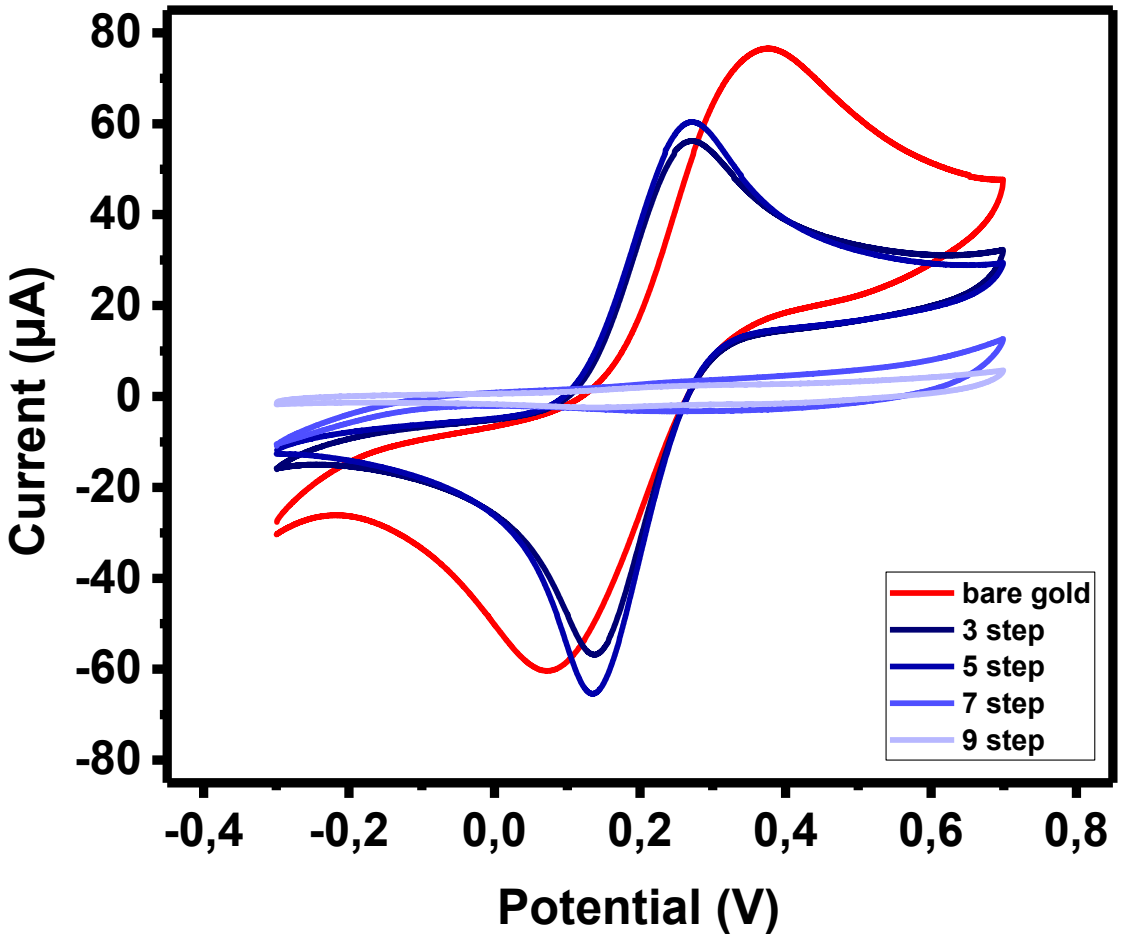

Figure 28. The cyclic voltammograms of bare gold electrode and polymer grafted gold electrodes with variable steps. The scan rate of 50 mV/s.

The 5 step nanogel grafted gold surface acid-base properties of the nanogel were examined by CV with $K_4Fe(CN)_6$ because of the pH independent redox process of ferrocyanide ion (

Figure 30).[83] While the acidity of the conditions increases, from neutral to an acidic environment, electron transfer is restricted but not blocked completely. Besides, the anodic/cathodic peak current is fourth times more than in the neutral medium.[29]

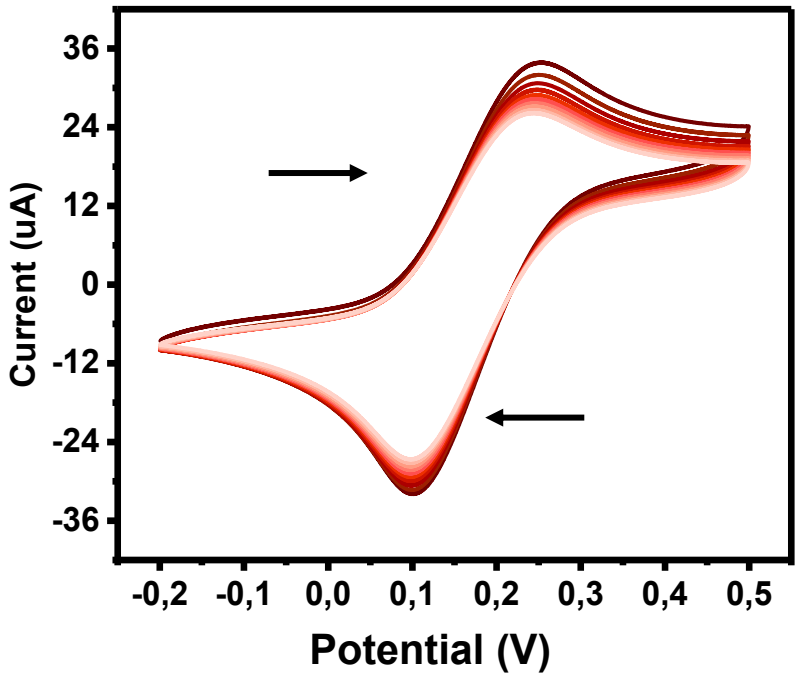

Figure 29. 5-step polymer grafted gold surface CV at 50 mV/s 0.01M PBS at 6.8 pH, 10 cycles.

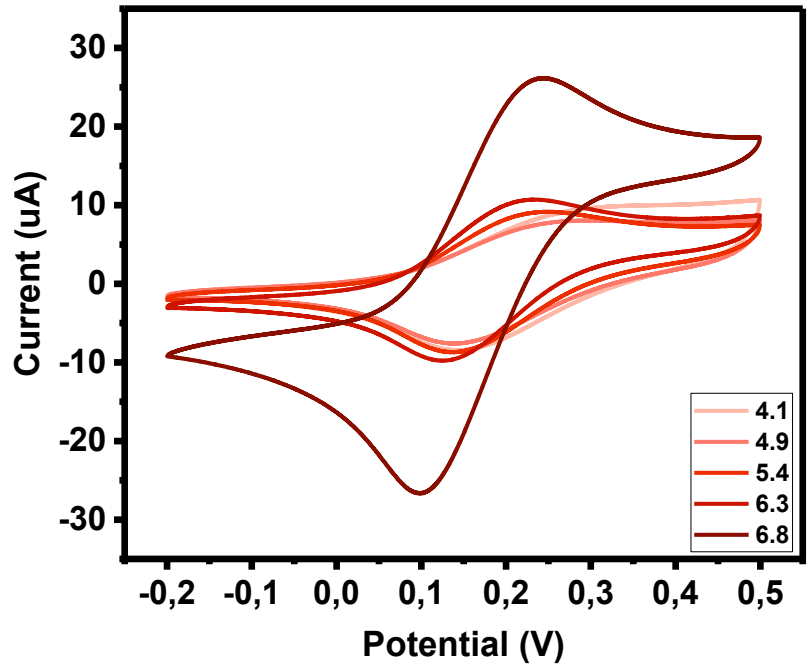

Figure 30. 5-step polymer grafted gold surface CV at 50 mV/s in 0.01M PBS of different pH.

Electrochemical impedance spectra were taken at 0V and in the 10^5 – 10^-1 Hz frequency range. The Nyquist representation of 5 step polymer grafted gold surface shown in Figure 31. EIS spectra fitted to Randles circuit which was consist of constant phase element (CPE), parallel connected charge transfer resistance (Rct), and series-connected open Warburg element (Wo); all in series with the active electrolyte resistance (Rsol). The incomplete semi-circle in the Nyquist plot was corresponding to capacitive behavior. The capacitance from constant phase element and resistance of charge transfer was calculated as;

$$C = R^{(1-n/n)} * Q^{(1/n)}.$$

The capacitance of the 5-step polymer grafted gold surface was found as 0.2736 Farad.

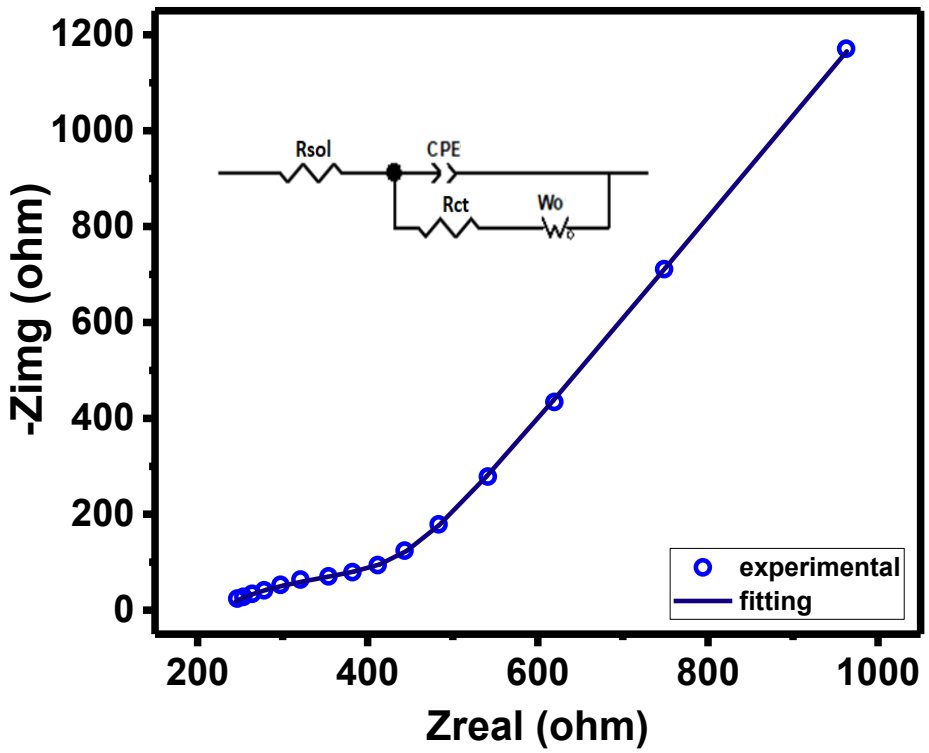

Figure 31. 5-step polymer grafted gold surface Nyquist's plot in presence of 1 mM $K_4[Fe(CN)_6]$ at pH 6.8.

3.1.1. Electroactive Nanogel Characterization

10% of Fc-BPEI. The 1H-NMR spectra in deuterated chloroform was compared with reference spectra which was taken from literature. 1H NMR (400 MHz, CDCl3): δ4.0-4.2 (Fc ring H), 3.5-3.4 (FcCH2-, NH), 2.2-2.9 (-CH2N-). The degree of substitution of the amine hydrogens by ferrocenylmethylene moieties was estimated from the integration ratio of the ferrocenyl proton to polymer methylene backbone signals in the 1H-NMR spectra of each resulting polymer and found to be 10% for the Fc-BPEI. [63]

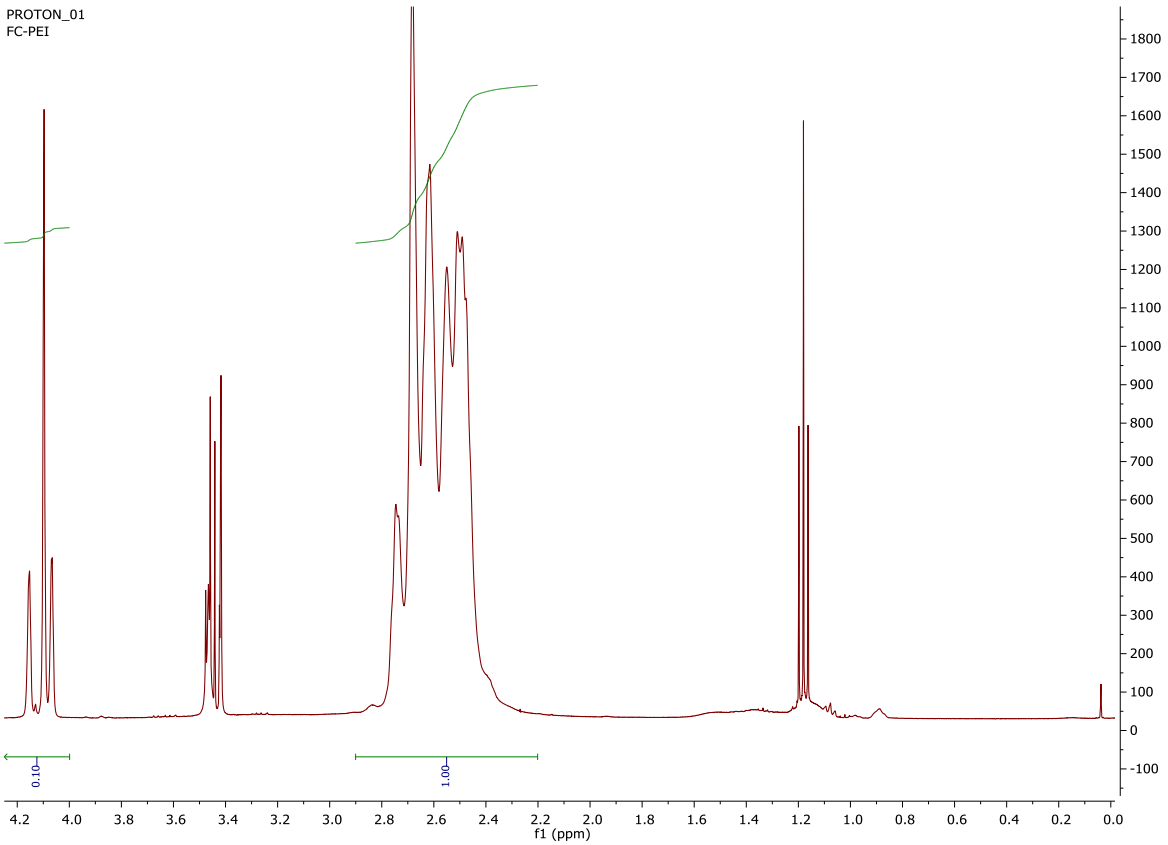

Figure 32. 1H-NMR spectra of ~10% substituted Fc-BPEI, in deuterated chloroform.

The AFM result of electroactive nanogel on gold surface that formed by using ferrocene carboxaldehyde (Fe) modified branched polyethyleneimine (BPEI) and Polyester scaffold (P1). AFM results showed that there are large aggregates and cloudy like structure globular formed homogeneous polymer domain on the surface and the

homogeneity of polymer regions is lower than the surface prepared by using BPEI. This inhomogeneous structure can be interpreted by the decrease in the number of functional groups of NH2 on Fc-BPEI that react with polymer scaffold (P1). The cross-section results of the electroactive nanogel and large aggregates nearly 5 times higher elevation than cloudy like structure globular formed homogeneous polymer. The result of the roughness of 40 μm² is 278.1 nm and it can be concluded that a smoother surface is obtained by using Fc-BPEI.

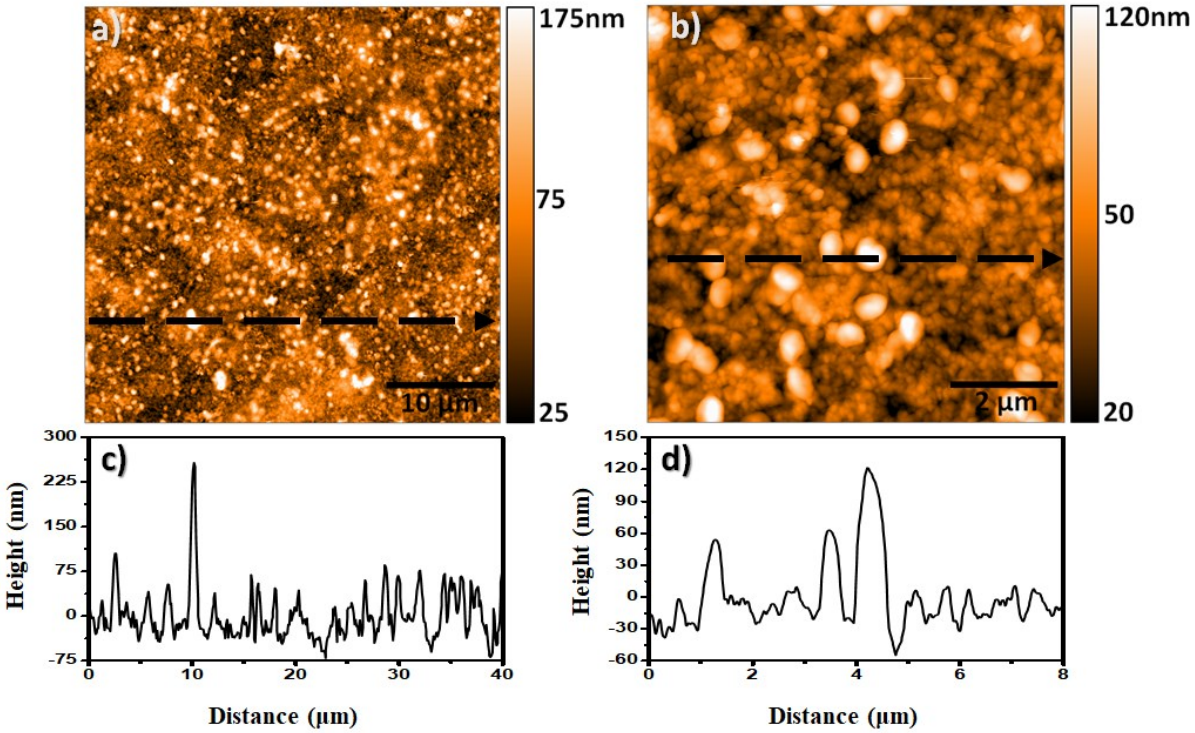

Figure 33. a, b) AFM topography images of 5-step polymer grafted gold electrode (ElectriCont-G), ferrocene carboxaldehyde (Fc) modified branched polyethyleneimine (BPEI) was used; c, d) cross-section of black dashed line respectively in a and b.

The cyclic voltammogram of electroactive nanogel, by providing covalent and selective pre-functionalization of ferrocene to provide electron transfer (ET) of the nanogels without needing an electrolyte. (Figure 34) While the scan rate decreases, the current density and peak separation is decreased too. The anodic peak current is 2.6 μA while the cathodic peak current is 1.5 μA. Hence, the easy and fast oxidation behavior of ferrocene was observed. (Figure 35)

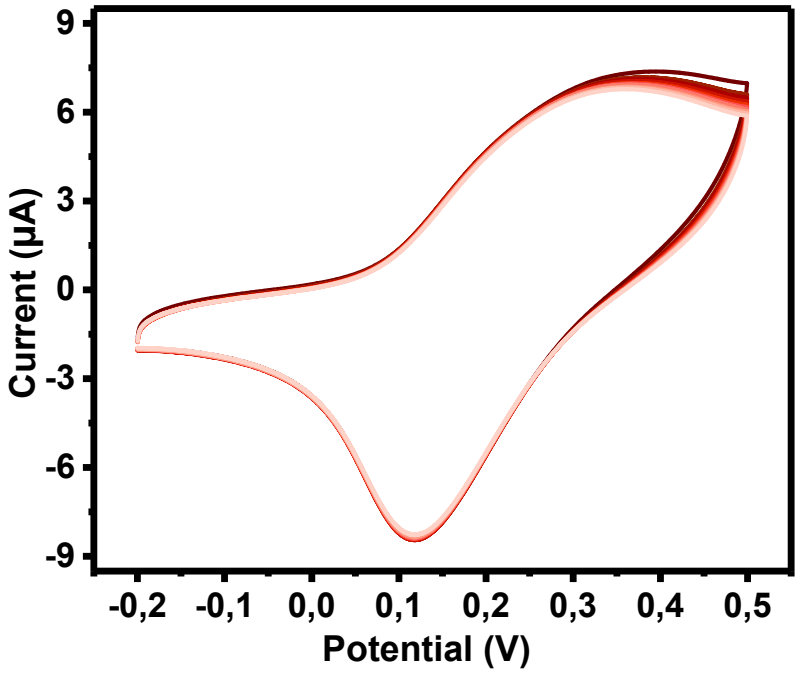

Figure 34. The cyclic voltammogram, 50mV/s scan rate, of 5-step Fc-BPEI post-functionalized with P1 polymer gold surface between -0,2V / 0,5V.

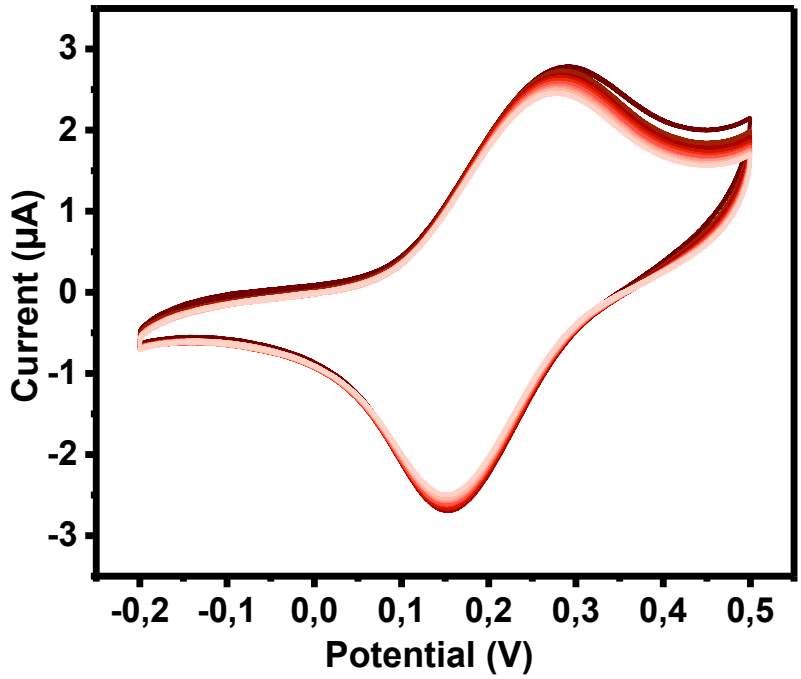

Figure 35. The cyclic voltammogram, 10mV/s scan rate, of 5-step Fc- BPEI post-functionalized with P1 polymer gold surface between -0,2V / 0,5V.

3.2. Characterization of Lithium-ion Conductivity of Gel

3.2.1. Characterization of Gel that consists of Branched Polyethyleneimine Gelator

Polyester scaffold (P1) based polymeric gel was produced by Aza-Michael addition reaction with branched polyethyleneimine (BPEI) and in the chloroform medium. The image of the freshly prepared gel is shown in Figure 36. The gel has a light-yellow color and a soft but solid-like structure. The gel also exhibits adhesive properties to the solid surface of the container.

Figure 36. Image of a Li+ ion gel with BPEI in chloroform medium.

The prepared polyester (P1) and branched polyethyleneimine (BPEI) based bulk gel is characterized by ATR-FTIR spectroscopy. The addition of BPEI proved by comparing dried gel and P1 polymer FTIR spectrums, as shown in Figure 37. The C=O stretching occurs at 1715 cm^{-1} and C-O-C asymmetric and symmetric stretching vibration gives signal at 1233 cm^{-1} and 1040 cm^{-1}. These stretching modes belongs the P1 polymer. The signal at 1573 cm^{-1} corresponds to incorporation of C=C stretching and N-H bending vibration of amines. The signal at 1145 cm^{-1} is refers the C-N stretching of amines. [80-82]

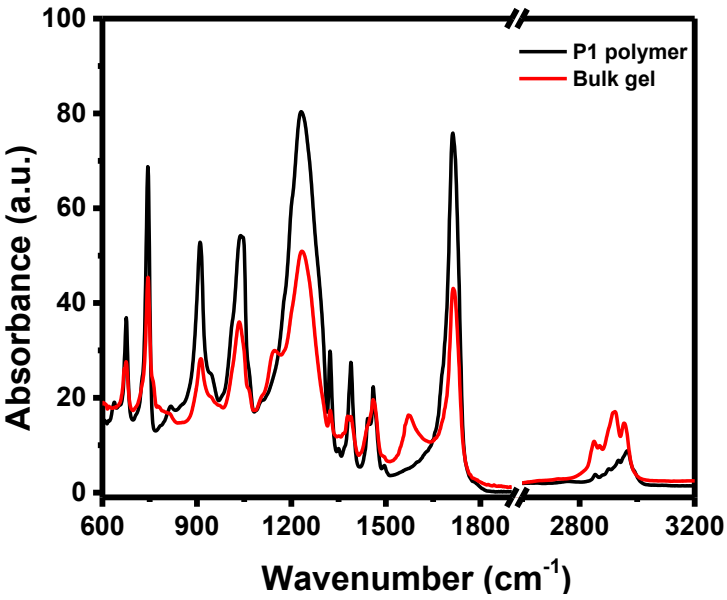

Figure 37. FTIR spectrum of P1 polymer and bulk gel.

Similar behaviors are observed between bulk gel and bulk gel containing lithium perchlorate salt. However, strong signals at 3521 cm^{-1} and 3569 cm^{-1} were observed. Lithium reacts readily with the moisture in the air to produce lithium hydroxide and hydrogen gas. Thus, these signals belong to the O-H stretching that typical due to the absorption of hydrogen bonds.[80, 84]

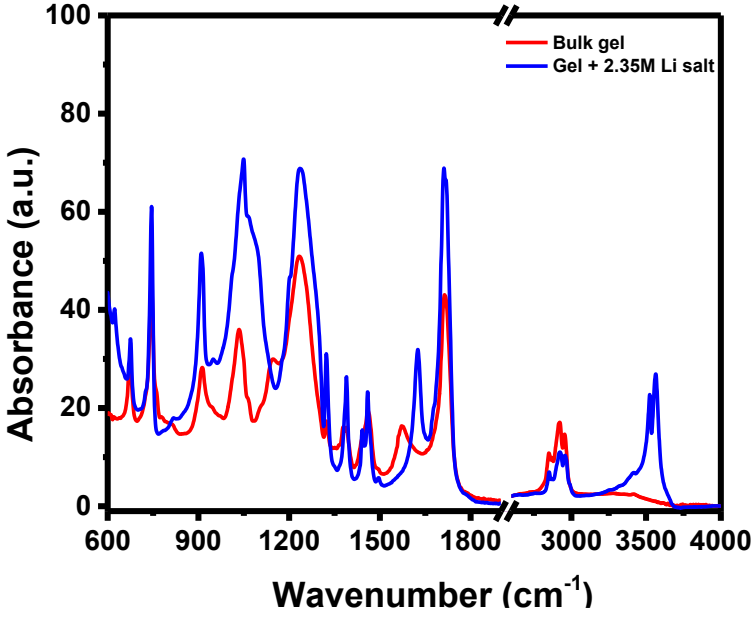

Figure 38. FTIR spectrum of bulk gel and bulk gel containing $LiClO_4$(2.35M).

The Lithium cations enters an interaction with the lone electron pairs of oxygen atoms in C=O and C-O-C groups of the polyester. The possible complexes are shown Figure 39.[85-87] This interaction of oxygen atoms and Li^+ ion leads to the dissociation of lithium perchlorate salt in the polymeric gel. The carbonyl group and lithium cation interactions are stronger that C-O-C groups in the ester molecules.[88]

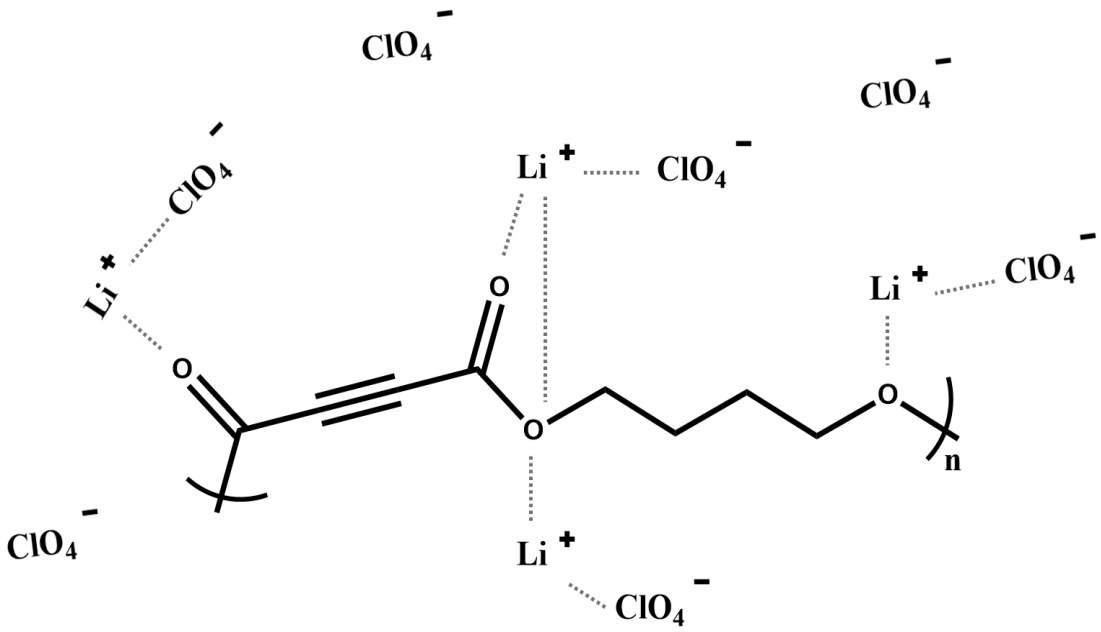

Figure 39. Schematic representations of the possible complexes form in Polyester / $LiClO_4$ system. Li+ ions coordinates with oxygen atoms. ClO^{4-} ions found as in "paired" or "free" form.

Figure 40 shows the positions of the absorption bands associated with the C–O–C bond of the ester group in the IR spectrum of both the gel and composites containing lithium perchlorate are nearly identical. However, the C-O-C symmetric stretching gets sharp and shifted to 1050 cm^{-1} from 1040 cm^{-1}, while broad shoulder at 1089 cm^{-1} associates with the asymmetric stretching of perchlorate (ClO_4^-) ion. Also, the signal at 622 cm^{-1} is responsible for the free ClO_4^- ion. The carbonyl (C=O) absorption is highly sensitive to the interaction behaviors.[86, 89] The signal at 1624 is responsible for the C=C bond observed instead of the signal at 1573 which corresponds to C=C conjugated C=O. By adding $LiClO_4^-$, carbonyl groups interact with Li^+ ion to form "Li^+ bonded C=O". Therefore, the carbonyl band at 1715 is broadened and gradually split into 1712 cm^{-1} and

1719 cm^{-1} that they responsible for "Li^+ free C=O". Also, the shoulder at 1676 cm^{-1} corresponds to the "Li^+ bonded C=O".[85, 87]

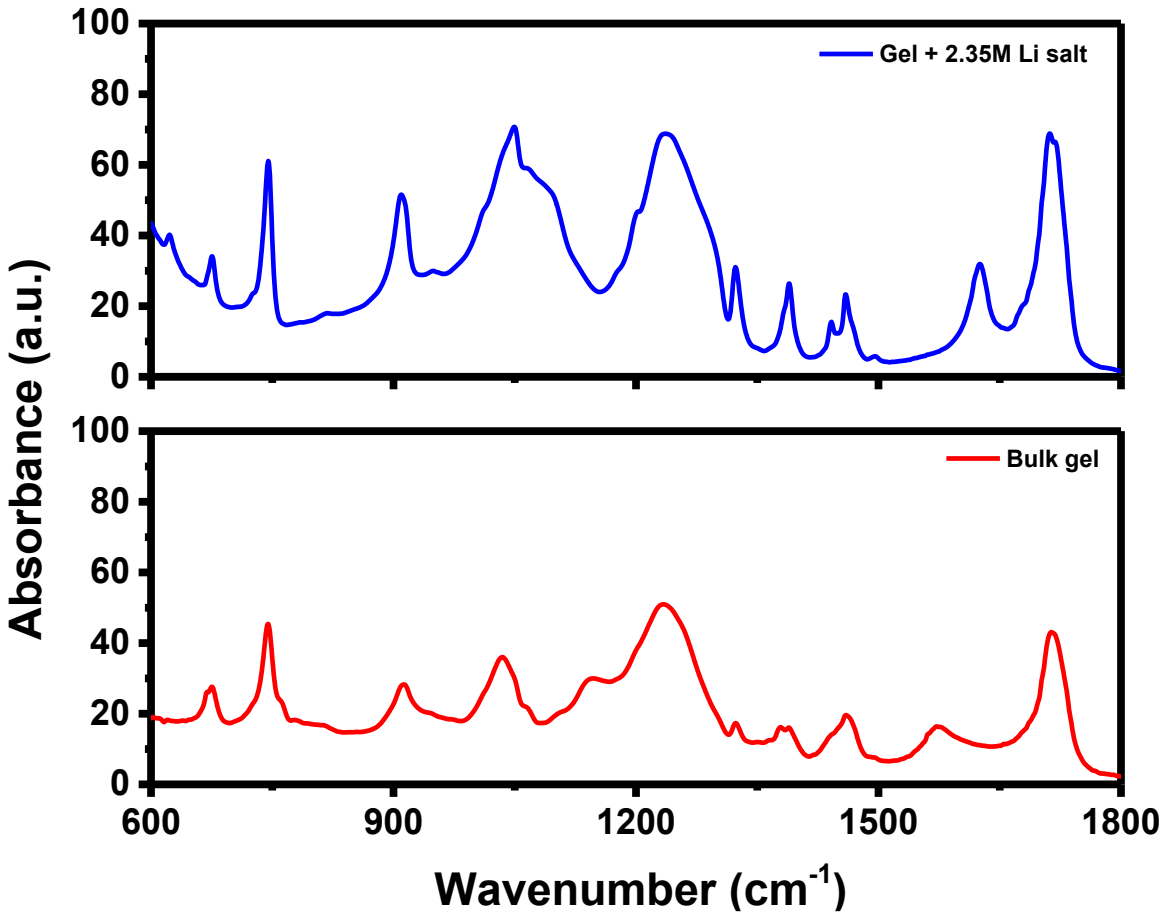

Figure 40. FTIR spectrum of bulk gel and bulk gel containing $LiClO_4$(2.35M).

As seen in Figure 41, there is no linear ratio between the electrical conductivity and the amount of salt. The values shown from the graph were taken instantly when the gel was removed from the solvent. The electrical conductivity drops rapidly in a tenth of a second. The solvent escape was remarkable in the case of gel electrolytes containing CHCl3 - EtOH mixtures. The escape of the solvent is causing a decrease in the ionic conductivity when the aprotic solvent phase in the only conductive phase in the structure of the gel.

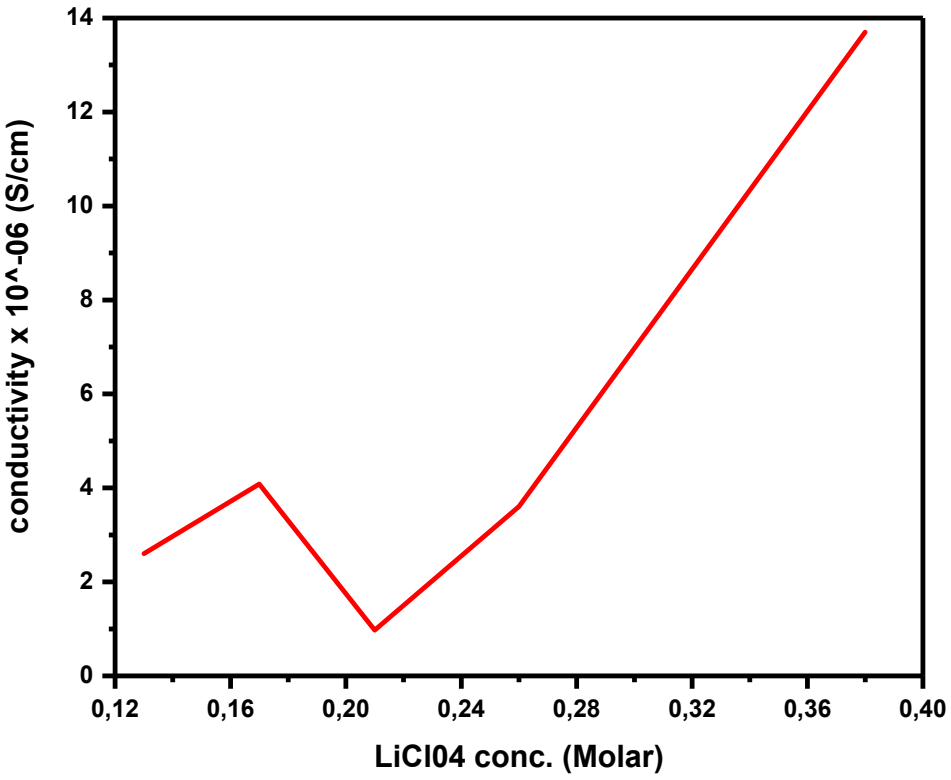

Figure 41. Electrical conductivity versus $LiClO_4$ concentration graph.

3.2.2. Characterization of Gel that consist of Ethylenediamine Gelator

The polyester-based polymeric gel was generated via low molecular weight gelator, ethylenediamine in propylene carbonate medium. The image of the gel and the gel containing lithium-ion are shown in Figure 42.

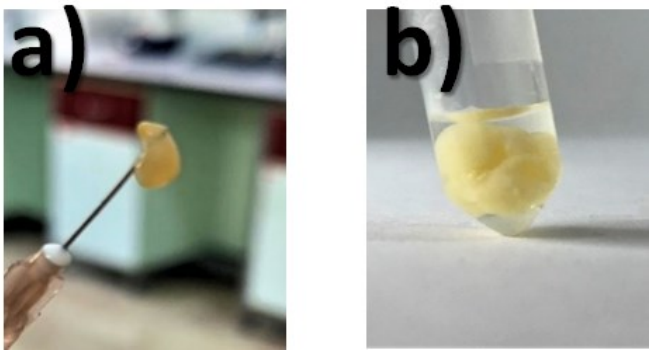

Figure 42. Images of a) bulk gel and b) bulk gel which contains 0.5M $LiClO_4$.

In Figure 43, the resistivity versus time comparison graph of gel and lithium-ion containing gel was shown. The lithium-ion gel resistance was approximately 200 kOhm and this corresponds to the conductivity of 2.5x10-5 S/cm. So, as expected, lithium-ion containing gel resistance was less than ion-free gel. Elapsed time also shows that the resistance of the lithium-ion gel was quite stable.

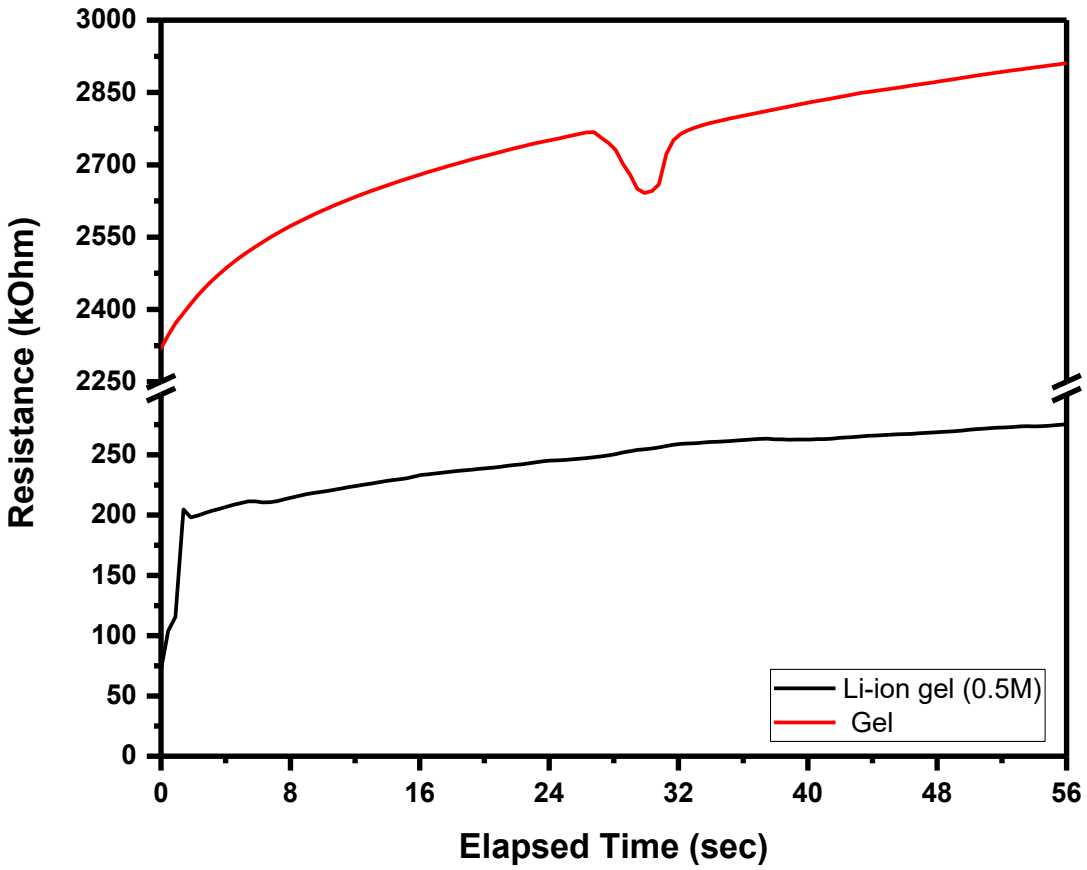

Figure 43. Resistivity vs Time comparison of bulk gel and bulk gel which contains 0.5M $LiClO_4$.

According to Table 2, the amount of ethylenediamine in the gelling medium was changed during P1 polymer and lithium salt content fixed. When two liquid gelators joined together, the solid-like gel was observed. So, the best gelling yield ratios were chosen as visually, 0.4%, 0.6%, 0.8%. The resistance was directly proportional to the ethylenediamine amount. When ethylenediamine concentration reaches the highest amount, that can gelated with P1 polymer, the resistance was the lowest and the

conductivity was highest. The increase in the amount of gelling increases the amount of liquid and salt that the gel can trap, so that the lowest resistance can be observed.

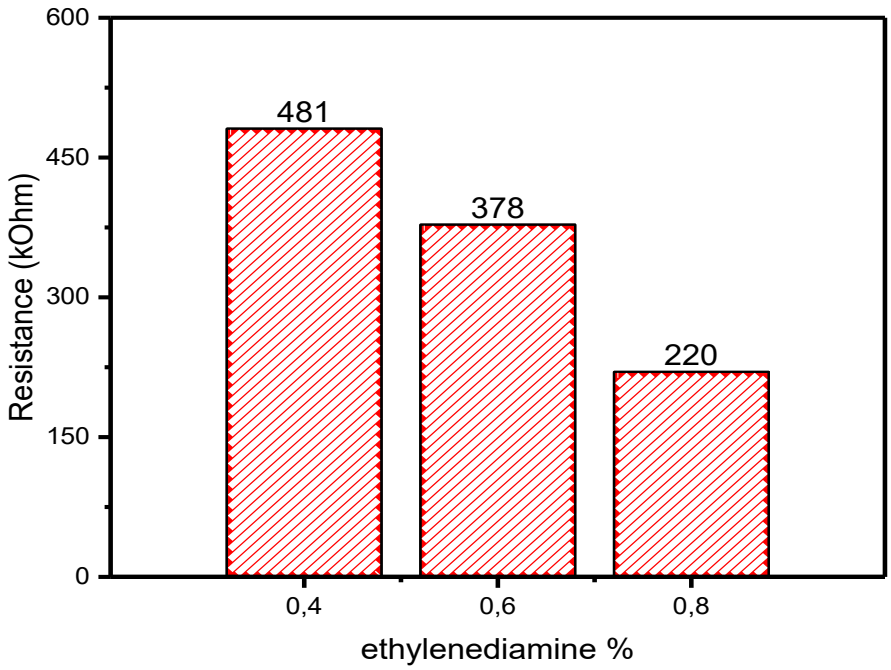

Figure 44. Resistivity change due to the ethylenediamine amount in gel

The general gelation amount determined based on visually the solid-like structure amount. In addition to this, the quantitative gelling degree calculated by the swelling degree equation. The crosslink density directly affects the degree of swelling. High crosslink density increases the swelling of the gel. The observation of an increase in the mass of swelled gel was expected because it will retain more liquid. The amount of gelling is influenced by the change in the slightest environmental impact. Accordingly, the gelation was repeated with the secondary amine ratios mentioned above and the approximate gelling ratio was compared from weighed before and after swelling of gel. (Figure 45) Then, we can say that the gelation ratio highest in the 0.8 % ethylenediamine content gel.

Figure 46, resistance measurements of gels which contains various amount of LiClO4 salt were done. The gelation was performed with the content of 0.8 % ethylenediamine. Electrical resistance decreased from the salt-free sample to the sample

containing 0.5 M LiClO4 salt. The measurement results were in the expected direction and electrical resistance decreased due to the increase in salt content.

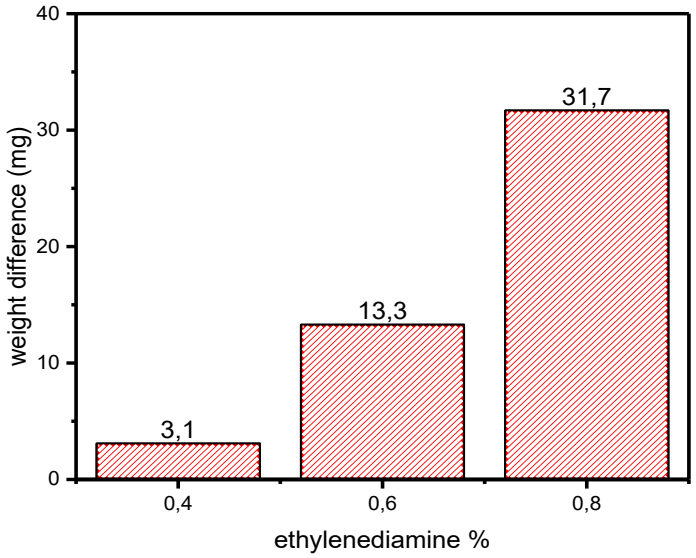

Figure 45. Gels swelling ratio due to the ethylenediamine amount in gel

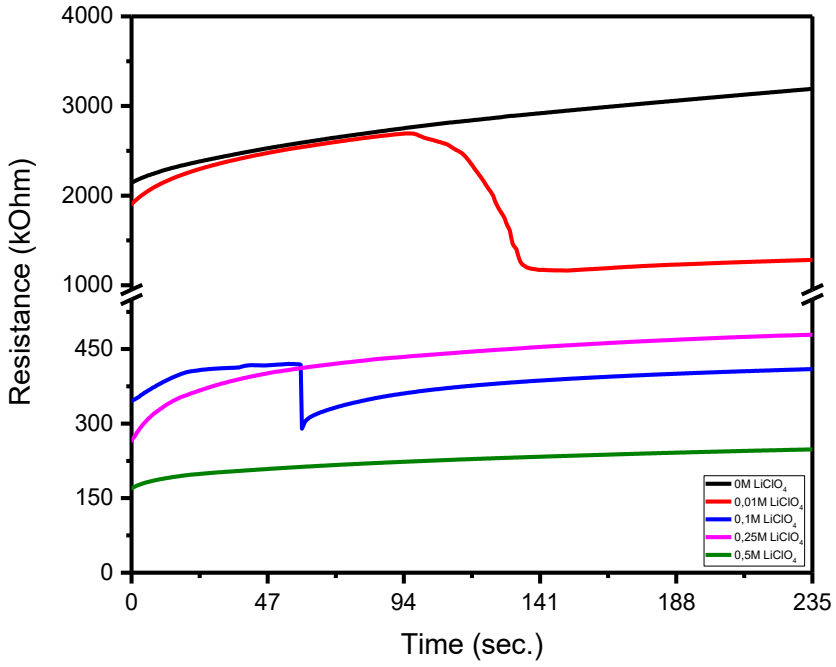

Figure 46. The graph shows the resistance of the gel which contains different amounts of $LiClO_4$ versus time in seconds.

CHAPTER 4

CONCLUSION

The general gel properties such as swelling, syneresis, and non-newtonian rheological behaviors gained an attractive position in many areas. According to requirements, the gel types are diversified. The polymeric gel is the most common one that combines both gel and polymer properties. Polymeric gels have a very distinctive property that originates from polymers' constitution, matrices, sizes, and the nature of the crosslinking. Besides, due to the polymeric gels tunable properties, they can be modified for energy storage, actuator, and sensor applications. In this study, electroactive polymer gels prepared by polyester scaffold gelator via secondary amine source in an organic solvent. Specially designed synthetic polyester has an easy synthesized procedure and accompanied it is easily accessible and cheap for commercial applications. Besides that, used polyester scaffold gives Aza-Michael addition reaction with secondary amine source laboriously and without need an initiator. Moreover, this reaction yields a gel in a short period, an average of 3 minutes. The two different secondary amine sources performed to increase the reaction yield and compliance of the gelation procedure environment, method, and different purposes. One of these reagents is branched polyethyleneimine which is a high molecular weight polymer that has many secondary amines in its backbone. The chloroform used as a common solvent for BPEI and P1 polymer. Secondly, a low molecular weight gelling agent ethylenediamine used because of its high solubility in propylene carbonate. Propylene carbonate is a favored non-volatile organic solvent for trapping lithium salt. Therefore, polyester-based organogel via ethylenediamine in propylene carbonate medium has higher lithium-ion conductivity than BPEI used gel in chloroform. To further increase conductivity, the mixture of PC and EC was used.

Applying gels to the surface or creating gel on the surface requires developing a completely different approach. There are different usage areas of gel coatings on the surface. But the most popular of these is sensor technologies. This is because the area studied in electrochemical biosensor applications is limited. With the use of electroactive gels, it is to obtain a wider active surface area than the surface area of the electrode and to increase the modular electron transfer rate. Also, it is to increase the capacity of the modified surface to hold the biological recognition element. In this study, gel formation

was achieved by using the grafting-from approach, one of the surface polymer grafting methods. Gold-coated surfaces, which are very popular in the biosensor field due to being an inert metal, were used as electrodes. Gold surfaces post-functionalized with isocyanate source and give strong bonding interactions. The nanometric polymer gel grafted on the post-functionalized surface via the sequential reaction of the polyester and BPEI. S As a result, the BPEI backbone has more NH2 groups and increases the reactive locations of the surface, especially for sensor applications. Electroactive polymer gel obtained by ferrocene modified BPEI. As a result, even in the absence of the electrolyte solution, the redox reaction of ferrocene was observed.

As a conclusion, polyester-based organogels were synthesized and characterized by using FTIR. Lithium-ion conductivity was calculated from resistance measurement by electronic multimeters. The electroactive polymeric gel was nanometrically and homogeneously synthesized on the gold surface. Polymeric gel grafted surface characterized by AFM, CV, and EIS.

REFERENCES

1. Salsamendi, M.; Rubatat, L.; Mecerreyes, D., Polymeric Ion Gels: Preparation Methods, Characterization, and Applications. In *Electrochemistry in Ionic Liquids*, Springer: 2015; pp 283-315.

2. Flory, P. In *Faraday Discussion*, Chem. Soc, 1974; pp 7-18.

3. Bacani, R.; Trindade, F.; Politi, M. J.; Triboni, E. R., *Nano Design for Smart Gels*. Elsevier Science: 2019.

4. Osada, Y.; Kajiwara, K., Gels handbook. Volume 1: The fundamentals. *Gels handbook. Volume 1: The fundamentals.* **2001**.

5. Pal, K.; Banerjee, I., *Polymeric gels: characterization, properties and biomedical applications*. Woodhead Publishing: 2018.

6. Hanabusa, K.; Suzuki, M., Development of low-molecular-weight gelators and polymer-based gelators. *Polymer Journal* **2014,** *46* (11), 776-782.

7. Cornwell, D. J.; Smith, D. K., Expanding the scope of gels–combining polymers with low-molecular-weight gelators to yield modified self-assembling smart materials with high-tech applications. *Materials Horizons* **2015,** *2* (3), 279-293.

8. Karoyo, A. H.; Wilson, L. D., Physicochemical properties and the gelation process of supramolecular hydrogels: A review. *Gels* **2017,** *3* (1), 1.

9. Sangeetha, N. M.; Maitra, U., Supramolecular gels: Functions and uses. *Chemical Society Reviews* **2005,** *34* (10), 821-836.

10. Truong, W. T.; Su, Y.; Meijer, J. T.; Thordarson, P.; Braet, F., Self-assembled gels for biomedical applications. *Chemistry–An Asian Journal* **2011,** *6* (1), 30-42.

11. Yan, J.; Wong, B. S.; Kang, L., Molecular Gels for Tissue Engineering. *Soft Fibrillar Materials* **2013**.

12. Yuan, C.; Guo, J.; Tan, M.; Guo, M.; Qiu, L.; Yan, F., Multistimuli responsive and electroactive supramolecular gels based on ionic liquid gemini guest. *ACS Macro Letters* **2014,** *3* (3), 271-275.

13. Ahn, S. K.; Ban, T.; Sakthivel, P.; Lee, J. W.; Gal, Y.-S.; Lee, J.-K.; Kim, M.-R.; Jin, S.-H., Development of dye-sensitized solar cells composed of liquid crystal embedded, electrospun poly (vinylidene fluoride-co-hexafluoropropylene) nanofibers as polymer gel electrolytes. *ACS applied materials & interfaces* **2012,** *4* (4), 2096-2100.

14. Xu, D.; Jin, J.; Chen, C.; Wen, Z., From nature to energy storage: a novel sustainable 3D cross-linked chitosan–PEGGE-based gel polymer electrolyte with excellent lithium-ion transport properties for lithium batteries. *ACS applied materials & interfaces* **2018,** *10* (44), 38526-38537.

15. Sahoo, S.; Kumar, N.; Bhattacharya, C.; Sagiri, S.; Jain, K.; Pal, K.; Ray, S.; Nayak, B., Organogels: properties and applications in drug delivery. *Designed monomers and polymers* **2011,** *14* (2), 95-108.

16. Suzuki, M.; Hanabusa, K., Polymer organogelators that make supramolecular organogels through physical cross-linking and self-assembly. *Chemical Society Reviews* **2010,** *39* (2), 455-463.

17. Carpi, F.; Mannini, A.; De Rossi, D., Dynamic splint-like hand orthosis for finger rehabilitation. *Biomedical applications of electroactive polymer actuators. John Wiley & Sons Ltd, New York* **2009**, 443-461.

18. Chen, H.; Ren, X.; Gao, G., Skin-Inspired Gels with Toughness, Antifreezing, Conductivity, and Remoldability. *ACS applied materials & interfaces* **2019,** *11* (31), 28336-28344.

19. Shi, Y.; Yu, G., Designing hierarchically nanostructured conductive polymer gels for electrochemical energy storage and conversion. *Chemistry of Materials* **2016,** *28* (8), 2466-2477.

20. Guyomard-Lack, A.; Delorme, N.; Moreau, C.; Bardeau, J.-F. o.; Cathala, B., Site-selective surface modification using enzymatic soft lithography. *Langmuir* **2011,** *27* (12), 7629-7634.

21. Lin, X.; Fukazawa, K.; Ishihara, K., Photoreactive polymers bearing a zwitterionic phosphorylcholine group for surface modification of biomaterials. *ACS applied materials & interfaces* **2015,** *7* (31), 17489-17498.

22. Liu, X.; Feng, Q.; Bachhuka, A.; Vasilev, K., Surface modification by allylamine plasma polymerization promotes osteogenic differentiation of human adipose-derived stem cells. *ACS applied materials & interfaces* **2014,** *6* (12), 9733-9741.

23. Tanaka, M.; Sawaguchi, T.; Kuwahara, M.; Niwa, O., Surface modification of silicon oxide with trialkoxysilanes toward close-packed monolayer formation. *Langmuir* **2013,** *29* (21), 6361-6368.

24. Lim, S.; Son, D.; Kim, J.; Lee, Y. B.; Song, J. K.; Choi, S.; Lee, D. J.; Kim, J. H.; Lee, M.; Hyeon, T., Transparent and stretchable interactive human machine interface based on patterned graphene heterostructures. *Advanced Functional Materials* **2015,** *25* (3), 375-383.

25. Wang, J.; Zhao, X.; Li, J.; Kuang, X.; Fan, Y.; Wei, G.; Su, Z., Electrostatic assembly of peptide nanofiber–biomimetic silver nanowires onto graphene for electrochemical sensors. *ACS Macro Letters* **2014,** *3* (6), 529-533.

26. Weng, Y.-H.; Xu, L.-T.; Chen, M.; Zhai, Y.-Y.; Zhao, Y.; Ghorai, S. K.; Pan, X.-H.; Cao, S.-H.; Li, Y.-Q., In Situ Monitoring of Fluorescent Polymer Brushes by Angle-Scanning Based Surface Plasmon Coupled Emission. *ACS Macro Letters* **2019,** *8* (2), 223-227.

27. Joh, D. Y.; McGuire, F.; Abedini-Nassab, R.; Andrews, J. B.; Achar, R. K.; Zimmers, Z.; Mozhdehi, D.; Blair, R.; Albarghouthi, F.; Oles, W., Poly (oligo (ethylene glycol) methyl ether methacrylate) Brushes on High-κ Metal Oxide Dielectric Surfaces for Bioelectrical Environments. *ACS applied materials & interfaces* **2017,** *9* (6), 5522-5529.

28. Ma, H.; Hyun, J.; Stiller, P.; Chilkoti, A., "Non-fouling" oligo (ethylene glycol)-functionalized polymer brushes synthesized by surface-initiated atom transfer radical polymerization. *Advanced Materials* **2004,** *16* (4), 338-341.

29. Marmisollé, W. A.; Capdevila, D. A.; de la Llave, E.; Williams, F. J.; Murgida, D. H., Self-assembled monolayers of NH2-terminated thiolates: order, p K a, and specific adsorption. *Langmuir* **2013,** *29* (17), 5351-5359.

30. Zhu, C.; Yang, G.; Li, H.; Du, D.; Lin, Y., Electrochemical sensors and biosensors based on nanomaterials and nanostructures. *Analytical chemistry* **2015,** *87* (1), 230-249.

31. Sechi, A.; Freitas, J. M.; Wünnemann, P.; Töpel, A.; Paschoalin, R. T.; Ullmann, S.; Schröder, R.; Aydin, G.; Rütten, S.; Böker, A., Surface-Grafted Nanogel Arrays Direct Cell Adhesion and Motility. *Advanced Materials Interfaces* **2016,** *3* (20), 1600455.

32. Jung, I. Y.; Kim, J. S.; Choi, B. R.; Lee, K.; Lee, H., Hydrogel based biosensors for in vitro diagnostics of biochemicals, proteins, and genes. *Advanced healthcare materials* **2017,** *6* (12), 1601475.

33. Karbarz, M.; Mackiewicz, M.; Kaniewska, K.; Marcisz, K.; Stojek, Z., Recent developments in design and functionalization of micro-and nanostructural environmentally-sensitive hydrogels based on N-isopropylacrylamide. *Applied Materials Today* **2017,** *9*, 516-532.

34. Li, L.; Shi, Y.; Pan, L.; Shi, Y.; Yu, G., Rational design and applications of conducting polymer hydrogels as electrochemical biosensors. *Journal of Materials Chemistry B* **2015,** *3* (15), 2920-2930.

35. Qu, F.; Zhang, Y.; Rasooly, A.; Yang, M., Electrochemical biosensing platform using hydrogel prepared from ferrocene modified amino acid as highly efficient immobilization matrix. *Analytical chemistry* **2014,** *86* (2), 973-976.

36. Freeman, M. H.; Hall, J. R.; Leopold, M. C., Monolayer-protected nanoparticle doped xerogels as functional components of amperometric glucose biosensors. *Analytical chemistry* **2013,** *85* (8), 4057-4065.

37. Azzaroni, O., Polymer brushes here, there, and everywhere: Recent advances in their practical applications and emerging opportunities in multiple research fields. *Journal of Polymer Science Part A: Polymer Chemistry* **2012,** *50* (16), 3225-3258.

38. Giussi, J. M.; Cortez, M. L.; Marmisollé, W. A.; Azzaroni, O., Practical use of polymer brushes in sustainable energy applications: interfacial nanoarchitectonics for high-efficiency devices. *Chemical Society Reviews* **2019,** *48* (3), 814-849.

39. Wang, S.; Wang, Z.; Li, J.; Li, L.; Hu, W., Surface-grafting polymers: from chemistry to organic electronics. *Materials Chemistry Frontiers* **2020**.

40. Zdyrko, B.; Luzinov, I., Polymer brushes by the "grafting to" method. *Macromolecular rapid communications* **2011,** *32* (12), 859-869.

41. Zhou, C.; Khlestkin, V. K.; Braeken, D.; De Keersmaecker, K.; Laureyn, W.; Engelborghs, Y.; Borghs, G., Solvent-controlled organization of self-assembled polymeric monolayers on gold: an easy approach for the construction of protein resistant surfaces. *Langmuir* **2005,** *21* (13), 5988-5996.

42. Stamm, M., Polymer surfaces and interfaces. *Characterization, Modification and Applications; Springer: Berlin, Germany* **2008**.

43. Edmondson, S.; Osborne, V. L.; Huck, W. T., Polymer brushes via surface-initiated polymerizations. *Chemical society reviews* **2004,** *33* (1), 14-22.

44. Conzatti, G.; Cavalie, S.; Combes, C.; Torrisani, J.; Carrere, N.; Tourrette, A., PNIPAM grafted surfaces through ATRP and RAFT polymerization: Chemistry and bioadhesion. *Colloids and Surfaces B: Biointerfaces* **2017,** *151*, 143-155.

45. Murugan, P.; Krishnamurthy, M.; Jaisankar, S. N.; Samanta, D.; Mandal, A. B., Controlled decoration of the surface with macromolecules: polymerization on a self-assembled monolayer (SAM). *Chemical Society Reviews* **2015,** *44* (10), 3212-3243.

46. Ngo, B. K. D.; Grunlan, M. A., Protein resistant polymeric biomaterials. ACS Publications: 2017.

47. Ozenler, S.; Sozen, Y.; Sahin, H.; Yildiz, U. H., Fabrication of post-functionalizable, bio-repellent, electroactive polyurethane interface on gold surface by Surface-Assisted (SurfAst) polymerization. *Langmuir* **2020**.

48. Zoppe, J. O.; Ataman, N. C.; Mocny, P.; Wang, J.; Moraes, J.; Klok, H.-A., Surface-initiated controlled radical polymerization: state-of-the-art, opportunities, and challenges in surface and interface engineering with polymer brushes. *Chemical reviews* **2017,** *117* (3), 1105-1318.

49. Yeow, J.; Chapman, R.; Gormley, A. J.; Boyer, C., Up in the air: oxygen tolerance in controlled/living radical polymerisation. *Chemical Society Reviews* **2018,** *47* (12), 4357-4387.

50. Bechler, S. L.; Lynn, D. M., Reactive polymer multilayers fabricated by covalent layer-by-layer assembly: 1, 4-conjugate addition-based approaches to the design of functional biointerfaces. *Biomacromolecules* **2012,** *13* (5), 1523-1532.

51. Hu, X.; Ji, J., Covalent layer-by-layer assembly of hyperbranched polyether and polyethyleneimine: multilayer films providing possibilities for surface functionalization and local drug delivery. *Biomacromolecules* **2011,** *12* (12), 4264-4271.

52. Richardson, J. J.; Cui, J.; Björnmalm, M.; Braunger, J. A.; Ejima, H.; Caruso, F., Innovation in layer-by-layer assembly. *Chemical reviews* **2016,** *116* (23), 14828-14867.

53. An, Q.; Huang, T.; Shi, F., Covalent layer-by-layer films: chemistry, design, and multidisciplinary applications. *Chemical Society Reviews* **2018,** *47* (13), 5061-5098.

54. Bergbreiter, D. E.; Liao, K.-S., Covalent layer-by-layer assembly—an effective, forgiving way to construct functional robust ultrathin films and nanocomposites. *Soft Matter* **2009,** *5* (1), 23-28.

55. Borges, J.; Mano, J. F., Molecular interactions driving the layer-by-layer assembly of multilayers. *Chemical reviews* **2014,** *114* (18), 8883-8942.

56. Kobayashi, S.; Müllen, K., *Encyclopedia of polymeric nanomaterials*. Springer Berlin Heidelberg: 2015.

57. Broderick, A. H.; Lynn, D. M., Covalent layer-by-layer assembly using reactive polymers. *Functional Polymers by Post-Polymerization Modification* **2013**, 371-406.

58. Sezen, H.; Suzer, S., XPS for chemical-and charge-sensitive analyses. *Thin Solid Films* **2013,** *534*, 1-11.

59. Mather, B. D.; Viswanathan, K.; Miller, K. M.; Long, T. E., Michael addition reactions in macromolecular design for emerging technologies. *Progress in Polymer Science* **2006,** *31* (5), 487-531.

60. Cetin, M.; Esen, C.; Daglar, O.; Luleburgaz, S.; Hizal, G.; Durmaz, H.; Tunca, U., 1, 3-Dipolar and Diels–Alder cycloaddition reactions on polyester backbones possessing internal electron-deficient alkyne moieties. *Polymer Chemistry* **2016,** *7* (46), 7094-7100.

61. Gunay, U. S.; Cetin, M.; Daglar, O.; Hizal, G.; Tunca, U.; Durmaz, H., Ultrafast and efficient aza-and thiol-Michael reactions on a polyester scaffold with internal electron deficient triple bonds. *Polymer Chemistry* **2018,** *9* (22), 3037-3054.

62. Ulman, A., *An Introduction to Ultrathin Organic Films: From Langmuir--Blodgett to Self--Assembly*. Academic press: 2013.

63. Merchant, S. A.; Glatzhofer, D. T.; Schmidtke, D. W., Effects of electrolyte and pH on the behavior of cross-linked films of ferrocene-modified poly (ethylenimine). *Langmuir* **2007,** *23* (22), 11295-11302.

64. MARKOWITZ, M. M.; HAWLEY, W. N.; BORYTA, D. A.; HARRIS, R. F., Lithium salts as solutes in nonaqueous media: solubility trends of lithium perchlorate. *Journal of Chemical and Engineering Data* **1961,** *6* (3), 325-327.

65. Li, T.; Balbuena, P. B., Theoretical studies of lithium perchlorate in ethylene carbonate, propylene carbonate, and their mixtures. *Journal of the Electrochemical society* **1999,** *146* (10), 3613-3622.

66. Nwokobia, F. U.; Cookey, G. A.; Abia, A. A., The Effect of Salt Concentration on the Conductivity and Viscosity of Binary Mixed Electrolyte Solutions.

67. Younesi, R.; Veith, G. M.; Johansson, P.; Edström, K.; Vegge, T., Lithium salts for advanced lithium batteries: Li–metal, Li–O 2, and Li–S. *Energy & Environmental Science* **2015,** *8* (7), 1905-1922.

68. Chen, H.; Fergus, J.; Jang, B., The effect of ethylene carbonate and salt concentration on the conductivity of propylene carbonate| lithium perchlorate electrolytes. *Journal of the electrochemical Society* **2000,** *147* (2), 399-406.

69. Thomas, S.; Thomas, R.; Zachariah, A. K.; Kumar, R., *Spectroscopic Methods for Nanomaterials Characterization*. Elsevier: 2017; Vol. 2.

70. Forghani, M.; McCarthy, J.; Mavroudis, H.; Donne, S. W., Electroanalytical characterization of electrochemical capacitor systems. *Electrochimica Acta* **2019,** *327*, 135010.

71. Nölle, R.; Beltrop, K.; Holtstiege, F.; Kasnatscheew, J.; Placke, T.; Winter, M., A reality check and tutorial on electrochemical characterization of battery cell materials: How to choose the appropriate cell setup. *Materials Today* **2020,** *32*, 131-146.

72. Privett, B. J.; Shin, J. H.; Schoenfisch, M. H., Electrochemical sensors. *Analytical chemistry* **2010,** *82* (12), 4723-4741.

73. Stradiotto, N. R.; Yamanaka, H.; Zanoni, M. V. B., Electrochemical sensors: a powerful tool in analytical chemistry. *Journal of the Brazilian Chemical Society* **2003,** *14* (2), 159-173.

74. Elgrishi, N.; Rountree, K. J.; McCarthy, B. D.; Rountree, E. S.; Eisenhart, T. T.; Dempsey, J. L., A practical beginner's guide to cyclic voltammetry. *Journal of Chemical Education* **2018,** *95* (2), 197-206.

75. Fuller, T. F.; Harb, J. N., *Electrochemical engineering*. John Wiley & Sons: 2018.

76. Mei, B.-A.; Munteshari, O.; Lau, J.; Dunn, B.; Pilon, L., Physical interpretations of Nyquist plots for EDLC electrodes and devices. *The Journal of Physical Chemistry C* **2018,** *122* (1), 194-206.

77. Randviir, E. P.; Banks, C. E., Electrochemical impedance spectroscopy: an overview of bioanalytical applications. *Analytical Methods* **2013,** *5* (5), 1098-1115.

78. Skoog, D.; Holler, F. J.; Crouch, S., Principles of Instrumental Analysis. Thomson Brooks. *Cole, Canada* **2007**.

79. Habibullah, H., 30 Years of Atomic Force Microscopy: Creep, Hysteresis, Cross-coupling, and Vibration Problems of Piezoelectric Tube Scanners. *Measurement* **2020,** *159*, 107776.

80. Socrates, G., *Infrared and Raman characteristic group frequencies: tables and charts*. John Wiley & Sons: 2004.

81. Stuart, B., Infrared spectroscopy. *Kirk-Othmer Encyclopedia of Chemical Technology* **2000**.

82. Thompson, J. M., *Infrared spectroscopy*. CRC Press: 2018.

83. Ghalkhani, M.; Maghsoudi, S., Development of an electrochemical differential pH sensing system based on mebendazole and potassium ferrocyanide. *Journal of Materials Science: Materials in Electronics* **2017,** *28* (18), 13665-13672.

84. Ebbing, D.; Gammon, S. D., *General chemistry*. Cengage Learning: 2016.

85. Lin, C.-K.; Wu, I.-D., Investigating the effect of interaction behavior on the ionic conductivity of Polyester/LiClO4 blend systems. *Polymer* **2011,** *52* (18), 4106-4113.

86. Sim, L.; Gan, S.; Chan, C.; Yahya, R., ATR-FTIR studies on ion interaction of lithium perchlorate in polyacrylate/poly (ethylene oxide) blends. *Spectrochimica Acta Part A: Molecular and Biomolecular Spectroscopy* **2010,** *76* (3-4), 287-292.

87. Wu, I.-D.; Chang, F.-C., Determination of the interaction within polyester-based solid polymer electrolyte using FTIR spectroscopy. *Polymer* **2007,** *48* (4), 989-996.

88. Dukhanin, G.; Dumler, S.; Sablin, A.; Novakov, I., Solid polymeric electrolyte based on poly (ethylene carbonate)-lithium perchlorate system. *Russian Journal of Applied Chemistry* **2009,** *82* (2), 243-246.

89. Abarna, S.; Hirankumar, G., Study on new lithium ion conducting electrolyte based on polyethylene glycol-p-tertoctyl phenyl ether and lithium perchlorate. *Int J ChemTech Res* **2014,** *6*, 5161-5167.